

NASA TECHNICAL NOTE

NASA TN D-6557



NASA TN D-6557

C.1

**LOAN COPY: RETURN TO
AFWL (DO NOT RETURN)
KIRTLAND AFB, NM**

01332208



TECH LIBRARY KAFB, NM

VIBRATION CHARACTERISTICS OF Z-RING-STIFFENED 60° CONICAL SHELL MODELS OF A PLANETARY ENTRY SPACECRAFT

by Eugene C. Naumann and John S. Mixson

Langley Research Center

Hampton, Va. 23365



0133208

1. Report No. NASA TN D-6557	2. Government Accession No.	3. Recipient's Catalog No.	
4. Title and Subtitle VIBRATION CHARACTERISTICS OF Z-RING-STIFFENED 60° CONICAL SHELL MODELS OF A PLANETARY ENTRY SPACECRAFT		5. Report Date December 1971	6. Performing Organization Code
		8. Performing Organization Report No. L-7381	10. Work Unit No. 114-08-05-04
7. Author(s) Eugene C. Naumann and John S. Mixson		11. Contract or Grant No.	
9. Performing Organization Name and Address NASA Langley Research Center Hampton, Va. 23365		13. Type of Report and Period Covered Technical Note	
		14. Sponsoring Agency Code	
12. Sponsoring Agency Name and Address National Aeronautics and Space Administration Washington, D.C. 20546		15. Supplementary Notes	
16. Abstract <p>An experimental investigation of the vibration characteristics of a 60° conical shell model of a planetary entry vehicle is described and the results presented. Model configurations include the shell with or without one or two Z-ring stiffeners and with or without a simulated payload.</p> <p>Tests were conducted with the model clamped at the small diameter and with the model suspended at the simulated payload. Additionally, calculated results obtained from application of several analytical procedures reported in the literature are presented together with comparisons between experimental and calculated frequencies and meridional mode shapes.</p> <p>Generally, very good frequency agreement between experimental and calculated results was obtained for all model configurations. For small values of circumferential mode number, however, the frequency agreement decreased as the number of ring stiffeners increased. Overall agreement between experimental and calculated mode shapes was generally good. The calculated modes usually showed much larger curvatures in the vicinity of the rings than were observed in the experimentally measured mode shapes.</p> <p>Dual resonances associated with modal preference were noted for the shell without Z-ring stiffeners, whereas the addition of stiffeners produced resonances for which the model responded in two or more modes over different sections of the shell length.</p>			
17. Key Words (Suggested by Author(s)) Structural dynamics Vibrations Ring-stiffened cones		18. Distribution Statement Unclassified - Unlimited	
19. Security Classif. (of this report) Unclassified	20. Security Classif. (of this page) Unclassified	21. No. of Pages 56	22. Price* \$3.00

VIBRATION CHARACTERISTICS OF Z-RING-STIFFENED 60° CONICAL SHELL MODELS OF A PLANETARY ENTRY SPACECRAFT

By Eugene C. Naumann and John S. Mixson
Langley Research Center

SUMMARY

An experimental investigation of the vibration characteristics of a 60° conical shell model of a planetary entry vehicle is described and the results presented. Model configurations include the shell with or without one or two Z-ring stiffeners and with or without a simulated payload.

Tests were conducted with the model clamped at the small diameter and with the model suspended at the simulated payload. Additionally, calculated results obtained from application of several analytical procedures reported in the literature are presented together with comparisons between experimental and calculated frequencies and meridional mode shapes.

Generally, very good frequency agreement between experimental and calculated results was obtained for all model configurations. For small values of circumferential mode number, however, the frequency agreement decreased as the number of ring stiffeners increased. Overall agreement between experimental and calculated mode shapes was generally good. The calculated modes usually showed much larger curvatures in the vicinity of the rings than were observed in the experimentally measured mode shapes.

Dual resonances associated with modal preference were noted for the shell without Z-ring stiffeners, whereas the addition of stiffeners produced resonances for which the model responded in two or more modes over different sections of the shell length.

INTRODUCTION

Space vehicles designed for entry into low-density planetary atmospheres require a low ratio of mass to frontal area so that sufficient deceleration forces are developed for a safe landing. This requirement (large area and low mass) can result in a relatively flexible structure. It is then possible that stresses, resulting from dynamic response to forces such as boundary-layer turbulence or from structural instabilities such as flutter, will be important in the design of the vehicle. Dynamic response and flutter analyses usually require knowledge of the natural vibration frequencies and mode shapes of the

vehicle. In many cases these space vehicles take the form of ring-stiffened truncated-cone shells. Until recently, little information was available on the frequencies and modes of wide-angle ring-stiffened conical shell configurations.

Vibration data for unstiffened, uniform thickness, isotropic conical shells are presented in references 1 to 5. The results of comparisons between calculated and measured vibration data, as presented in these references, indicate that the vibration behavior of simple unstiffened conical shells is adequately understood. Some recent research on the vibrations of ring-stiffened conical shells is reported in references 6 to 10. These references report comparisons between experimental and calculated data which vary from poor to very good.

The present experimental investigation was undertaken to provide additional data (1) for 60° conical shells with up to three flexible, widely spaced rings and (2) for conical shells having a large mass attached to simulate a payload. In addition, the free rings were also tested. Concurrent with the experimental investigation, results became available from several analytical investigations in which different mathematical representations were used to approximate the ring-stiffened conical shell. These analytical procedures are found in references 9 to 12.

The paper has two main purposes: first, to describe the experimental investigation and present the results; and second, to compare calculated results obtained from the different analytical procedures with the test results. Additionally, the results of analytical studies dealing with various techniques of representing ring-to-shell attachments are presented. The data are presented in a manner which facilitates comparisons between the experimental and calculated results.

SYMBOLS

Any consistent system of units may be used in these analyses.

A_R	ring cross-sectional area
E	Young's modulus
E_C, E_R	Young's modulus of shell and ring, respectively
E_1, E_2	Young's modulus in meridional and circumferential directions, respectively
EA	extensional stiffness of ring

EI_1	bending stiffness of ring about ξ_1 -axis
EI_3	bending stiffness of ring about ξ_3 -axis
EI_{13}	bending stiffness of ring due to coupling between bending about ξ_1 - and ξ_3 -axes
$E\Gamma_3$	warping parameter
G_R	shear modulus of ring
GJ	torsional stiffness of ring
h	total thickness of shell wall
h_1, h_2	shell thickness from inner and outer surface to reference surface, respectively
$I_{1,R}, I_{2,R}$	moments of inertia of ring
$I_{S,R}$	moment of inertia of ring about \hat{s} -axis
$I_{Sz,R}$	product of inertia of ring with respect to \hat{s} - and \hat{z} -axes
$I_{z,R}$	moment of inertia of ring about \hat{z} -axis
J_R	torsional constant of ring
$J_{e,R}$	polar moment of inertia of ring cross section
m	order of occurrence in spectrum of modes having the same circumferential mode number n
m_1	mass of ring per unit circumferential length
n	number of circumferential waves in mode shape
r	radius of shell measured in plane normal to shell axis

r_1, r_2	shell minimum and maximum radii, respectively
S	tensile strength
s	meridional coordinate
s_0	meridional distance to shell minimum radius
s_R	meridional distance to ring attachment circumference
\hat{s}_R	meridional distance from \hat{z} -axis to ring centroid
w	normal displacement component
z	normal distance from shell reference surface to ring attachment circumference
z_R	distance from shell middle surface to ring centroid
δ	semivertex angle of shell
Γ_R	ring warping constant
$\left. \begin{matrix} \epsilon_1, \epsilon_2, \epsilon_3, \\ \overline{\epsilon}_1, \overline{\epsilon}_2 \end{matrix} \right\}$	element lengths (figs. 4(c) and 4(d))
μ	Poisson's ratio
ρ	mass density
ρ_c	mass density of shell
ρ_R	mass density of ring
ϕ	shell circumferential coordinate

A circumflex over a symbol denotes a function evaluated at the attachment circumference.

EXPERIMENTAL INVESTIGATION

Test Configurations

The models used in this investigation were composed of several discrete parts which were tested in various combinations. Figure 1 is an exploded schematic view of the various components in their relative locations. Identified in figure 1 are: shell, nose plug, two Z-ring stiffeners, and simulated payload and its supports.

The shell was fabricated from 0.0635-cm-thick 6061-T6 aluminum-alloy sheet. The shell was formed by rolled halves joined with machine-welded butt joints oriented along shell generators. The variation in sheet thickness was on the order of ± 0.0013 cm (± 2 percent).

The nose plug, Z-rings, and simulated payload were machined from a 3.08-cm-thick 6061-T6 aluminum-alloy plate. The plate was large enough to allow the largest ring to be machined in one piece. The simulated payload was supported on four 1.27-cm-diameter aluminum-alloy rods evenly spaced on a 10.16-cm-diameter circle. The nose plug and two Z-rings were attached to the shell with commercially available epoxy bonding material and 0.3175-cm-diameter positive-lock blind rivets spaced 2.54 cm center to center. This method of attachment was used to insure a minimum of local shell distortion. The simulated payload was fastened to the support rods through bolts (not shown) which screwed into the ends of the rods. The support rods were fastened to the plate section of the nose plug with threaded studs to facilitate removing the payload for several sets of tests.

Table I presents the listed mechanical properties for the material used in the model components as well as the mass of the components and assemblies. It should be noted that the component mass is for the component after the rivet holes had been drilled and that the fastener mass includes the bonding material and rivet.

Figure 2 presents a tabulation of the different model configurations and the boundary supports for each configuration. The model configurations are designated by the numbers 1, 2, and 3 according to the number of ring stiffeners attached to the shell. Thus, configuration 1 is obtained by attaching the base ring at the shell small diameter; configuration 2 is obtained by attaching a Z-ring stiffener at the large diameter of configuration 1; and configuration 3 is obtained by attaching a Z-ring stiffener at the shell midspan of configuration 2. For each model configuration one or more of three support conditions were imposed on the model small diameter. The large diameter of the shell was always unsupported (free). The three support conditions and the designation used are as follows: C designation, clamped with the nose plate alone held in the fixture; \bar{C} designation, clamped with both the nose plate and the base ring held in the fixture; and S designation, simulated payload attached to the nose plate and the model softly suspended at the

simulated payload. Thus, model configuration 2S refers to a model composed of the shell, nose plug, large Z-ring, and simulated payload, suspended at the simulated payload. The sketches in figure 2 schematically represent the model configuration and boundary support and are used where appropriate in subsequent figures to assist in associating the model configuration with the data. A description of the model small-diameter supports follows.

Clamped support.- A clamped boundary support was obtained by clamping the small end of the shell and/or nose plug between two machined fittings. Two sets of fittings were fabricated; one set had a 10.16-cm radius and the other set, a 7.62-cm radius. (See nose plug detail in fig. 1.) The larger set was used for model configuration 1C̄ and is shown in figure 3(a). The smaller set of fittings was used for model configurations 1C, 2C, and 3C. Clamping force was applied by a 2.54-cm-diameter bolt passing through the center of the fittings into a large mass. (See fig. 3(b).)

Suspended support.- The suspended boundary support was obtained by suspending the model at the payload with soft springs, as shown in figure 3(c). This method of suspension was used for model configurations 1S and 2S. The model-suspension system had measured spring-mass frequencies of less than 1 Hz for rotational, swinging, and vertical motions.

Free boundary supports for tests of the Z-ring stiffeners were simulated by suspending the rings on eight soft elastic springs. The springs were attached with tabs located at equal intervals around the ring circumference.

Test Procedures

Test procedures, used in this investigation, are generally the same as those described in detail in reference 9. The following is a brief description of the test procedures with emphasis on procedures applicable only to this investigation.

Excitation.- In general, two types of shakers were used. An air shaker (ref. 13) was used to excite the lower frequency modes of the shell and of the rings (frequency less than 100 hertz). A small (6.7-newton) electrodynamic shaker was used to excite the higher frequency modes. For these tests the electrodynamic shaker was attached to the model with a small vacuum cup, and was driven with the amplified output of a variable-frequency oscillator. The frequency ranges of the two shaker systems were overlapped to insure a smooth transition in frequency.

During the course of this investigation, the results obtained on the ring-stiffened shell indicated that in certain frequency bands, modal coupling was occurring. (See later discussion.) In an attempt to define the modal behavior in these frequency bands better, two of the small electrodynamic shakers were employed simultaneously to excite the

model. The shakers were driven by amplified sinusoidal signals generated by a dual-channel variable-frequency oscillator (see ref. 14), which permitted the excitation of the model with two shakers by using the same frequency source but with the capability to vary the phase of one shaker relative to the other.

For all the models it was difficult to excite modes for which the circumferential wave number is equal to zero (axisymmetric modes) and modes for which the circumferential wave number is equal to 1. For models 1S and 2S special techniques were employed to try to excite these modes. The test setup used for $n = 1$ modes is illustrated in figure 3(c). As shown, the 6.7-newton electrodynamic shaker was fastened mechanically to the simulated payload and normal to the model center line. (The model shown in fig. 3(c) to illustrate the procedure is not one of the models discussed in this paper.) The test setup used for $n = 0$ modes is illustrated in figure 3(d). A higher force capacity (11.2-newton) electrodynamic shaker was placed, as shown, to drive directly along the model center line. The shaker was fastened mechanically to the center of the base plate.

Motion sensors.- The displacements of the vibrating model were determined by using a noncontacting displacement probe shown in figure 3(a) and described in reference 15. The servo-controlled probe and track system allow continuous recording of deflections along a meridian or circumference. Accelerometers were mounted on the simulated payload, nose plug, and rings for models 1S and 2S. (See fig. 3(c).)

Resonance detection and identification.- The usual method of model resonance detection was to observe the output of the displacement probe as the excitation frequency was slowly varied. When a model resonance was detected, the frequency was held constant while the mobile survey apparatus was used to obtain the mode shape. In general, the mode shape was measured along three circumferences and one meridian. The experimentally obtained mode shapes were used to define a set of mode numbers, n and m , for each model resonance. The circumferential mode number n generally denotes the number of circumferential waves in the mode shape and the meridional mode number m denotes the order of occurrence in the spectrum of modes having the same circumferential mode number n . For the free rings the index m was assigned the value zero for the lowest mode; for all other configurations the index m was assigned the value 1 for the lowest mode. When mode numbers were assigned for resonances in which modal superposition occurred, the procedure described in reference 9 was used.

METHODS OF ANALYSIS

Because of the interest in the general class of structures involving ring-stiffened conical shell segments and in view of the variations in agreement between experimental and calculated frequencies and mode shapes as reported in the literature, it was deemed

of interest to compare the experimental results of this investigation with the results obtained from the application of several different analyses. To this end, the analytical procedures of references 9, 10, 11, and 12 (hereinafter called methods 9, 10, 11, and 12, respectively) were selected as representative of current technology. Methods 9, 10, and 11 were applied to model configurations 1C, 2C, 3C, and $1\bar{C}$, and method 12 was applied to model configuration 1S. The following sections provide a brief résumé of each method, the assumptions used in applying the method, and the computer inputs used.

Method 9

The basic shell is represented by using the Novozhilov thin-shell theory. A ring is represented as an assembly of an arbitrary number of shell segments which can be connected in various ways to form such sections as Z-sections and I-sections. The Novozhilov theory is also used to represent each of the shell segments making up the rings. In this representation each shell segment is free to stretch, bend, twist, and warp independently within the constraints imposed by the Novozhilov theory, those imposed by connections to other ring segments, and those imposed by connections of the ring to the basic shell. To obtain approximate numerical solutions for vibration modes, a Rayleigh-Ritz procedure is employed, in which the three (middle surface) displacements of the basic shell and the three displacements of each ring segment are expanded in independent polynomial series.

The connections among shell segments representing the rings, the connections between the rings and the basic shell, and the constraints provided by supports are specified by directly writing the appropriate equations of constraint. This procedure allows the ring to be connected to the shell along any number of circumferential lines and it allows for specification of compatibility between any combination of displacements and rotations on a connection line. It also allows for specification of axisymmetric rigid support constraints at any location in the system.

For this investigation, method 9 was applied to the free rings and to model configurations 1C, $1\bar{C}$, 2C, and 3C. Model component idealizations are shown schematically in figure 4(a) and the program input parameters are presented in table II(a). As shown in figure 4(a), the Z-rings were approximated with three short shell segments. For example, to represent the small Z-ring, ring 2 is attached to ring 2A and ring 2A is attached to ring 2B. The approximated Z-ring was attached to the shell by attaching one segment (ring 2 for the small Z-ring) to the shell. For all attachments between adjacent ring segments, one attachment circumference was assumed and compatibility was enforced among the three displacements and the rotation about the circumferential direction. The attachments between the rings and shell were varied.

Method 10

The basic shell is represented by using the Sanders thin-shell theory. The Rayleigh-Ritz procedure is used in the analysis of the basic shell with polynomial expansions of the three middle-surface displacements. The rings are handled in the manner set forth by McElman in reference 16. Effects of stretching, bending, twisting, and warping are accounted for. The connection between a ring and the basic shell is limited to one attachment circumference and compatibility is enforced among the three displacements and the rotation about the circumferential direction. The method is specialized for shells having clamped-free boundary conditions. For the purposes of this paper, the results denoted in reference 10 as "with ring secondary stiffness" are applicable. Figure 4(b) and table II(b), abstracted from reference 10, present the model idealizations and program input parameters used to apply this method to model configurations 1C, $1\bar{C}$, 2C, and 3C.

Method 11

This method is applicable to shells of revolution with general meridional curvature. As in method 9, the shell theory used is the Novozhilov thin-shell theory. Finite elements are used in the numerical analysis of the basic shell. The elements are "geometrically exact," in that each element has the exact shape of the section of the shell covered by the element. The displacements in an element are represented by third-order polynomials in the inplane displacements and by fifth-order polynomials in the normal displacement. Compatibility at nodes is maintained between the displacements, the first derivatives of the displacements, and the second derivative of the normal displacement. Any combination of axisymmetric rigid-support constraints can be applied at the ends of the basic shell. A ring is represented by using conventional approximations; that is, the ring section is assumed to undergo a planar deformation and a warping deformation. The planar deformation accounts for stretching, twisting, and bending about two mutually perpendicular axes. The warping deformation is taken to be an arbitrarily specified function multiplied by the twist. Ring to shell attachments are limited to one attachment circumference per interface (must coincide with a node of the basic shell) with compatibility enforced among three displacements and the rotation about the circumferential direction.

Model component idealizations used to apply this method to the free rings and model configurations 1C, $1\bar{C}$, 2C, and 3C are shown schematically in figure 4(c) and program input parameters are presented in table II(c). A difficulty in applying method 11 is that a completely rational procedure is not available for specifying the warping function. This point is discussed in references 11 and 12. The procedure described in reference 11 was followed in the applications of this paper. In this procedure the warping function is assumed to be zero in all calculations except the calculation of $E\Gamma_3$ appearing in

table II(c). In calculating $E\Gamma_3$ the warping function used is, in effect, that predicted by St. Venant torsion theory for straight bars.

Method 12

This method is applicable to rotationally symmetric bodies having a nonaxisymmetric elastic-mass system attached at points. The method involves a linear superposition of the modes of the model elements, modal coupling occurring as a result of enforcing attachment point compatibility (as opposed to circumferential line compatibility for rings in methods 9, 10, and 11). This method was applied to model configuration 1S by using the idealized model components and program input parameters shown in figure 4(d). The general analysis scheme was as follows:

(1) By using method 11, free-free modes were calculated for the shell-base ring combination and for the plate section of the nose plug

(2) The results of scheme (1) were coupled by requiring compatibility of displacements and rotations at junction 3 (fig. 4(d)) of the plate and junction 1 of the shell-base ring

(3) The simulated payload and supports were idealized and lead to the following stiffness and mass matrices: (a) payload contributed mass only (infinitely rigid) and (b) the support rods contributed stiffness matrix elements obtained from beam bending theory. (Each support rod was assumed to be massless and infinitely rigid in extension and torsion.)

(4) The combined model modes and frequencies were determined by using 45 modes of the shell-base-plate combination obtained in scheme (2) when $n = 0, 1, 2, \dots, 14$; $m = 0, 1, \text{ and } 2$ and by using the payload and support stiffness and mass matrices obtained in scheme (3).

RESULTS AND DISCUSSION

In the following sections the experimental and calculated results of this investigation are presented and discussed, and applicable comparisons are made. To facilitate presentation, the results are grouped as follows: (1) free rings; (2) models without Z-ring stiffeners (model configurations 1C, $1\bar{C}$, and 1S); (3) models with one Z-ring stiffener (model configurations 2C and 2S); (4) model with two Z-ring stiffeners (model configuration 3C); and (5) additional results and discussion related to analytical procedures. In general, the data are presented and discussed in the following sequence: frequency, mode shapes, and boundary effects.

Free Rings

The experimental and calculated frequency results are presented in table III and in figure 5. In figure 5 the experimental results are represented with symbols and the calculated results with lines faired through the discrete values. Although the three methods of analysis yield slightly different results, it would appear that each method adequately predicts the bending frequencies of the rings. Method 9 gives the most precise agreement with experiment.

Models Without Z-Ring Stiffeners

Frequency.- The experimental and calculated frequency results for model configurations 1C, $1\bar{C}$, and 1S are presented in table IV and figure 6. In figure 6, the experimental results are represented with symbols and the calculated results with lines faired through the discrete values. The occurrence of two slightly different frequencies, for the same mode number, in the experimental results is in agreement with vibration characteristics noted in unstiffened shells. (See, for example, ref. 17.) In the present test results, the dual resonances follow a pattern in which the frequency spread for odd values of n is approximately twice that of the even values of n . An examination of the experimental circumferential mode shapes (not shown) indicated that the higher frequency corresponded to a mode orientation for which antinodes occurred at the shell fabrication seams and that the lower frequency corresponded to a vibration mode orientation for which nodes occurred at the seams. Thus, the dual resonances correspond to modal orientation preferences for which the relative rotation of the mode is one-fourth of the mode wavelength. It is also of interest to note that a ring at the small diameter (model configurations 1C and 1S) tended to suppress dual resonances for values of n less than 7.

Excellent agreement is obtained between the experimental and calculated frequencies for model configurations 1C, 1S, and $1\bar{C}$ (figs. 6(a), 6(b), and 6(c), respectively). For the clamped-free, unstiffened shell (configuration $1\bar{C}$), essentially identical frequencies were obtained from each of the three analytical procedures for all values of n . For model configuration 1C, the three procedures yielded essentially the same frequencies for values of n greater than 4 but gave small differences for values of n less than 4. The small differences in frequency between the three analyses, for small values of n , are attributed to differences in analytical concept and idealizations of the base-ring-shell structure. (See fig. 4.)

The circumferential mode shapes calculated by method 12 for configuration 1S exhibited only very slight indications of modal coupling (one n mode was very dominant for each calculated resonance) between different n values. This result is in agreement with experimental data for which modal coupling was not observed. This lack of modal

coupling (coupling was expected because of the point connections of the simulated payload mass) was probably due to the "smearing" effect of the very stiff plate section of the nose plug.

Mode shapes.- Experimental and calculated, normalized meridional mode shapes for model configuration 1C are presented in figures 7(a) and 7(b), respectively. With the exception of small variations near the base ring (normalized shell length, zero) for small values of n , the calculated mode shapes were the same for each of the analytical methods. These small differences are attributed to the differences in model component idealizations. A comparison between figures 7(a) and 7(b) indicates very good agreement between experimental and calculated mode shapes. One noticeable trend which occurs for values of n greater than 9 is that the measured mode shapes (fig. 7(a)) exhibit increasing amounts of negative (downward) motion for normalized shell lengths less than 0.5, whereas the calculated shapes (fig. 7(b)) show no deflection in the same region.

Boundary effects.- Boundary support effects are readily evaluated from a comparison of the experimental frequency results for model configurations 1C and 1S shown in figure 8, where the clamped boundary (configuration 1C) represents a conceptual spacecraft launch support condition and the suspended boundary (configuration 1S) represents a spacecraft entry condition. In figure 8, the symbols represent experimental frequencies and the curves are faired through the data to facilitate visualization. As can be seen, the effect of boundary supports is appreciable for small values of n ($n \leq 3$) and negligible for $n \geq 4$.

Models with One Z-Ring Stiffener

Frequency.- Experimental frequency results for model configurations 2C and 2S and calculated results for model configuration 2C are presented in table V. Figure 9 gives a plot of the results for model configuration 2C. Dual resonances associated with modal orientation preferences were not observed for these model configurations. However, modal coupling (that is, at a given frequency, the model was observed to vibrate in two or more modes over various sections of the model length) was present in most of the resonances measured. Additionally, several sets of these coupled resonances occurred within a narrow frequency band and made mode identification difficult. In such frequency ranges (for example, 115 to 130 Hz), two phased electrodynamic shakers were used (appropriately in or out of phase) in an attempt to uncouple the modes and to isolate the predominant mode. Although this procedure did result in accentuation of participating modes and made identification in many cases much less difficult, it was not possible to excite experimentally some of the modes predicted by analysis. This condition is reflected by the missing experimental points in figure 9. The results shown in table V are the frequencies at which a given modal response was the strongest and/or the mode shapes were the clearest. The

complex modal coupling is consistent with the experience reported in reference 9 for similar model configurations. Attempts were made, by using the 11.2-newton shaker (fig. 3(d)), to excite axisymmetric resonances in model configuration 2S but no clear mode shapes were discernible.

For model 2C very good frequency agreement is obtained between the experimental results and the calculated results for each method. Comparisons of results obtained from the three analysis methods show small frequency variations, which are probably due to model component idealizations and/or attachment geometry assumptions. (See subsequent discussion in the section on attachment geometry.)

Mode shapes.- Selected normalized experimental and calculated meridional mode shapes for model configuration 2C are presented in figures 10(a) and 10(b), respectively. The experimental mode shapes which are presented were selected for minimum modal coupling. The calculated mode shapes are consecutive over a range of $n = 2$ to $n = 9$ to illustrate trends in mode shape behavior. Visual comparisons between associated mode shapes in parts (a) and (b) of figure 10 indicate that each of the analytical methods predicts the general shape of the measured mode in the meridional direction although the local shell curvature, in the vicinity of the rings, generally is much greater in the calculated modes than in the experimental modes. In many cases in which the Z-ring is oscillating, the mode shapes differ considerably for the various methods of analysis. The calculated frequencies of these modes also differ, as shown in figure 9. The characteristic change in meridional mode shape, from maximum motion at the ring to no motion at the ring ($n = 3, m = 1$ to $n = 6, m = 1$ and $n = 5, m = 2$ to $n = 8, m = 2$), and the corresponding changes in the curves of frequency plotted against circumferential mode number shown in figure 9 are in agreement with observations of similar model configurations reported in reference 9.

Boundary effects.- Experimental frequency results for the clamped and suspended boundary conditions of configurations 2C and 2S are shown in figure 11, where the symbols represent the experimental first mode ($m = 1$) frequencies. The lines are faired through the data to aid in visualization. The boundary support at the model small diameter is seen in figure 11 to have some effect on the frequency for n less than 6; that is, the suspended boundary condition (configuration 2S) results in somewhat lower frequencies than does the clamped boundary condition (configuration 2C). This trend is the same as previously discussed for the models without Z-ring stiffeners (configurations 1C and 1S).

Model With Two Z-Ring Stiffeners

Frequency.- Experimental and calculated frequency results for the clamped spacecraft with two Z-rings (configuration 3C) are presented in table VI and plotted in figure 12. In the experimental investigation, the occurrence of resonances associated with coupled

modes was much more pronounced (that is, wider frequency bands) than that discussed for model configuration 2C. Additionally, the coupling was much more complex; that is, for many resonances three or four modes were evident over various parts of the shell length. Application of two electrodynamic shakers had very little effect when used in an attempt to isolate predominant modes. The results presented in table VI are for resonances at which modal coupling was minimum.

Comparisons (fig. 12) of experimental frequencies and frequencies calculated by different methods indicate that appreciable differences are obtained for the first mode ($m = 1$), and large differences are obtained for the second mode. In view of the generally good agreement obtained for the other model configuration, this poor agreement for model configuration 3 indicates that some facet of the ring-to-shell attachment is not properly treated. Thus none of the analytical methods adequately represents the essential effects of the small Z-ring attached at the shell midlength.

Mode shapes. - Experimentally obtained normalized meridional mode shapes are presented in figure 13(a), and calculated normalized meridional mode shapes are presented in figure 13(b).

Although there is not a one-to-one correspondence in mode shapes between figures 13(a) and 13(b) and several modes from method 10 were not available, obvious similarities in shape and trends can be noted between the experimental and calculated mode shapes for $m = 1$. For this model configuration no clear, uncoupled, experimental mode shapes were obtained for the $m = 2$ modes.

Differences between calculated mode shapes and measured mode shapes are, in general, associated with local shell curvatures in the vicinity of a ring. Likewise differences between calculated mode shapes (fig. 13(b)) are also associated with local shell curvatures and can be shown to be associated with differences in calculated frequency.

Discussion Related to Analytical Procedures

Effect of attachment geometry. - Attachment geometry, as used herein, refers to the mathematical model used to represent the attachment interface between the shell and ring. Formulation of the attachment geometry requires that both the number and location of attachment circumferences within the interface be selected, and that the compatibility equations between shell and ring displacements and rotations at the attachment be selected. Effects of attachment geometry variations reported in reference 9, for models similar to the models used in this study, show that both the number of attachments and the constraint equations assumed for each attachment can have an appreciable effect on frequency and mode shape. Additionally, the study indicated that the location of the ring along the shell (that is, at an end or in the interior) had an effect on the sensitivity of the results to the attachment geometry.

To evaluate the effects of attachment geometry assumptions, two parametric studies were conducted for model configuration 3C. In the first study the method of reference 9 was used to evaluate the effect of the number of equations used at the small Z-ring attachment, and the effect of varying the representation of the boundary (that is, attaching a free ring to a clamped shell or a free shell to a clamped ring). In the second study the method of reference 11 was used to evaluate the effect of the location of the attachment circumference in the shell-ring interface.

The frequency results of the parametric studies are presented in table VII and plotted in figure 14. Meridional mode shapes obtained for the different attachment geometries are presented in figure 15.

By considering first the frequencies calculated by the analysis of reference 9, table VII(a), and figure 14(a), it can be seen that the degree of constraint (that is, three equations – solid line in figure 14(a); or four equations – short dashed line in figure 14(a)) assigned to the Z-ring located at midshell length has a moderate effect on the first-mode frequencies and a pronounced effect on some second-mode frequencies. On the other hand, the details of the attachment of the shell or ring to the fixed boundary have only small effects on the calculated frequencies (that is, ring clamped – short dashed line in fig. 14(a); or shell clamped – short-dash—long-dash line in figure 14(a)). By considering now the frequencies calculated by the analysis of reference 11, table VII(b), and figure 14(b), it can be seen that the point within the shell-ring interface at which compatibility is forced likewise has a moderate effect on the first-mode frequencies and a pronounced effect on some second-mode frequencies. It is of interest to note the similarity – shape and frequency value – between the solid curves of figure 14(a) and the dashed curves of figure 14(b), and also the dashed curves of figure 14(a) and the solid curves of figure 14(b). Thus ring-to-shell attachments can be selected so that different methods of analysis would yield the same frequency results, although the geometries themselves were quite different. This result suggests a deficiency in the analytical representations and thus a need for additional research.

Calculated meridional mode shapes are presented in figures 15(a) and 15(b) for the analyses of methods 9 and 11, respectively. Each figure shows that changes in the attachment geometry cause some changes in the mode shape for all values of n , although the most significant changes correspond to values of n for which motion is occurring at an attachment. The mode shapes which show appreciable change generally correspond to n values which also show appreciable frequency change. A comparison of figures 15(a) and 15(b) indicates that both analyses predict essentially the same behavior in the vicinity of the large Z-ring whereas the mode shapes from reference 9 consistently have less curvature in the vicinity of the small Z-ring.

Ring effects.- Two interesting effects associated with rings are observed when comparing frequency curves for models having different combinations of rings and when comparing frequency curves for models having rings which are considerably different in size and shape. The effect of rings on the frequency curves is shown very clearly in figure 16, where the calculated first mode ($m = 1$) frequencies of model configurations 1C, 2C, and 3C are presented. A comparison of the curves for model configurations 1C and 2C show that adding a Z-ring stiffener at the shell large diameter has little effect for $n = 0, 1, \text{ and } 2$; the frequency curves rapidly diverge to a maximum separation at $n = 5$; and then the frequency separation remains essentially constant. A comparison of the curves for model configurations 2C and 3C shows a somewhat different trend. For this comparison, the rapid divergence in frequencies peaks at $n = 7$, after which the frequency differences due to the addition of a Z-ring at the shell midspan slowly subside until at $n = 15$ the frequency difference is small. The peak-frequency increase due to the small Z-ring ($n = 7$ for configurations 2C and 3C) was approximately 1.6 times as big as the peak-frequency increase due to the large Z-ring ($n = 5$ for configurations 1C and 2C).

The second facet of the effects of rings can be seen in figure 17. In figure 17, the calculated frequencies for model configuration 2C (solid line, method 9) are presented together with the calculated frequencies for model configuration 4 of reference 9 (dashed curve). The only difference between the two model configurations is the character of the ring stiffener attached at the shell large diameter. Although the rectangular ring of reference 9 is more massive (greater than 2:1) than the Z-ring of the present investigation, both models have essentially the same curves of frequency against mode number.

CONCLUDING REMARKS

The results of an experimental investigation of the vibration characteristics of a Z-ring-stiffened, 60° conical shell model of a planetary entry spacecraft, together with the calculated results obtained from the application of several methods, available in the literature, support the following observations:

Frequency comparisons between the experimental and calculated results generally yielded very good agreement over a wide range of frequency and mode number. The poorest agreement between experimental and calculated frequencies resulted when the rings were moving with large amplitudes compared with areas of the shell between rings. This condition occurred only for small values of the circumferential wave number n . In this mode range, agreement between experimental and calculated frequencies decreased as the number of rings increased. Corresponding comparisons between measured and calculated mode shapes showed generally good overall shape agreement. The calculated mode shapes for small values of n consistently produced more local shell curvature in the vicinity of rings than was evident in the measured mode shapes.

Notable differences between frequencies and mode shapes obtained from three different methods of analysis also generally occurred for small values of n . These differences in calculated values appear to be related to the sensitivity of the analytical results to ring-to-shell attachment assumptions.

Two types of modal behavior were observed in the experimental investigation. The first type, for models without Z-ring stiffeners, involved preferred mode orientations with slightly separated resonant frequencies. The second type, for models with Z-ring stiffeners, involved coupled modes for which the model responded in two or more modes over various parts of its length at a single resonance. The number of modes involved in the modal coupling increased as the number of ring stiffeners was increased.

Experimental frequencies obtained from tests in which the model was clamped at the shell small diameter were found, for small values of n , to be slightly higher than frequencies obtained when the model was suspended from the simulated payload. No differences were noted for higher n values.

Langley Research Center,
National Aeronautics and Space Administration,
Hampton, Va., October 26, 1971.

REFERENCES

1. Naumann, Eugene C.: On the Prediction of the Vibratory Behavior of Free-Free Truncated Conical Shells. NASA TN D-4772, 1968.
2. Lindholm, Ulric S.; and Hu, William C. L.: Non-Symmetric Transverse Vibrations of Truncated Conical Shells. *Int. J. Mech. Sci.*, vol. 8, no. 9, Sept. 1966, pp. 561-579.
3. Seide, Paul: On the Free Vibrations of Simply Supported Truncated Conical Shells. *Israel J. Technol.*, vol. 3, no. 1, Feb. 1965, pp. 50-61.
4. Weingarten, V. I.: Free Vibrations of Conical Shells. *J. Eng. Mech. Div., Amer. Soc. Civil Eng.*, vol. 91, no. EM 4, Aug. 1965, pp. 69-87.
5. Swaney, Thomas George: Free Vibration of Conical Shells. Ph. D. Diss., Kansas State Univ., 1967.
6. Weingarten, V. I.: Free Vibrations of Ring-Stiffened Conical Shells. *AIAA J.*, vol. 3, no. 8, Aug. 1965, pp. 1475-1481.
7. Crenwelge, Otto E., Jr.; and Muster, D.: Free Vibrations of Ring-and-Stringer-Stiffened Conical Shells. *J. Acoust. Soc. Amer.*, vol. 46, no. 1, July 1969, pp. 176-185.
8. Godzevich, V. G.; and Ivanova, O. V.: Free Oscillations of Circular Conical and Cylindrical Shells Reinforced by Rigid Circular Ribs. NASA TT F-291, 1965.
9. Naumann, Eugene C.; Catherines, Donnell S.; and Walton, William C., Jr.: Analytical and Experimental Studies of Natural Vibration Modes of Ring-Stiffened Truncated-Cone Shells With Variable Theoretical Ring Fixity. NASA TN D-6473, 1971.
10. Sewall, John L.; and Catherines, Donnell S.: Analytical Vibration Study of a Ring-Stiffened Conical Shell and Comparison With Experiment. NASA TN D-5663, 1970.
11. Adelman, Howard M.; Catherines, Donnell S.; Steeves, Earl C.; and Walton, William C., Jr.: User's Manual for a Digital Computer Program for Computing the Vibration Characteristics of Ring-Stiffened Orthotropic Shells of Revolution. NASA TM X-2138, 1970.
12. Steeves, Earl C.; Durling, Barbara J.; and Walton, William C., Jr.: A Method for Computing the Response of a General Axisymmetric Shell With an Attached Asymmetric Structure. *AIAA Structural Dynamics and Aeroelasticity Specialists Conference and the ASME/AIAA 10th Structures, Structural Dynamics, and Materials Conference*, Apr. 1969, pp. 302-328.
13. Herr, Robert W.: A Wide-Frequency-Range Air-Jet Shaker. NACA TN 4060, 1957.

14. Schoenster, James A.; and Clary, Robert R.: Experimental Investigation of the Longitudinal Vibration of a Representative Launch Vehicle With Simulated Propellants. NASA TN D-4502, 1968.
15. Naumann, Eugene C.; and Flagge, Bruce: A Noncontacting Displacement Measuring Technique and Its Application to Current Vibration Testing. Preprint No. 16.18-5-66, Instrum. Soc. Amer., Oct. 1966.
16. McElman, John A.: Eccentrically Stiffened Shallow Shells. Ph. D. Thesis, Virginia Polytech. Inst., 1966.
17. Mixson, John S.: Experimental Modes of Vibration of 14° Conical-Frustum Shells With Free Ends. NASA TN D-4428, 1968.

TABLE I.- PROPERTIES AND MASSES OF MODEL COMPONENTS

[Shell and components fabricated from 6061-T6 aluminum alloy]

Tensile strength, S , GN/m ²	0.310
Young's modulus, E , GN/m ²	68.95
Poisson's ratio, μ	0.315
Mass density, ρ , kg/m ³	2.715

Component	Mass, kg	Total component mass, ¹ kg
Shell (free-free)	2.290	2.290
Nose plug	0.735	} 0.739
Fasteners	0.004	
Ring 2	0.358	} 0.370
Fasteners	0.012	
Ring 1	0.626	} 0.655
Fasteners	0.029	
Payload	2.880	} 3.316
Payload supports	0.408	
Fasteners	0.028	
Maximum model mass		7.370

¹Component mass is net after fastener holes have been drilled. Fasteners include total mass of rivets and bonding material.

TABLE II.- PROGRAM INPUT PARAMETERS

(a) Analysis method 9

Component	Shell	Ring 1	Ring 2	Ring 2A	Ring 2B	Ring 3	Ring 3A	Ring 3B
Minimum radius, cm	7.620	7.544	34.726	33.988	34.021	60.126	59.388	59.421
Maximum radius, cm	60.960	10.084	35.509	35.451	34.800	60.909	60.851	60.200
Semivertex angle, deg	60	60	60	150	60	60	150	60
Thickness, cm	0.0635	0.2413	0.1321	0.1321	0.1321	0.1321	0.1321	0.1321
Modulus, GN/m ²	68.95	68.95	68.95	68.95	68.95	68.95	68.95	68.95
Poisson's ratio	0.315	0.315	0.315	0.315	0.315	0.315	0.315	0.315
Mass density, kg/m ³	2.715	2.715	2.715	2.715	2.715	2.715	2.715	2.715
Terms per displacement series	12	3	4	4	4	3	3	3
Shell-ring attachments ¹	-----	1	1	0	0	1	0	0
Ring-ring attachments ²	-----	0	0	1	1	0	1	1
Equations of constraint ³	-----	4	3	4	4	4	4	4
Boundary conditions ⁴	f-f	c-f	f-f	f-f	f-f	f-f	f-f	f-f

¹Number of attachment circumferences per interface between the shell and ring.

²Number of attachment circumferences per interface between two ring segments.

³Number of equations of constraint per attachment (3 = 3 displacements; 4 = 3 displacements and 1 rotation).

⁴First designation is for component small diameter; second designation is for component large diameter;

f indicates free; c indicates clamped.

TABLE II.- PROGRAM INPUT PARAMETERS – Continued

(b) Analysis method 10

Conical shell:

r_1 , including base ring, mm	76.2
r_2 , cm	60.96
E_C , GN/m ²	68.95
h , mm	0.635
δ , deg	60
μ	0.315
ρ_C , kg/m ³	2.715

Rings:

E_R , GN/m ²	68.95
G_R , GN/m ²	26.2
ρ_R , kg/m ³	2.715

Property	Base ring	Z-ring	
		Attached to shell	Free
s_R , mm	102.7	699 406	694.0 401.3
\hat{s}_R , mm	0	4.166	0
z_R , mm	-1.587	-15.3	0
A_R , mm ²	74.5	61.6	61.6
$I_{S,R}$, cm ⁴	0.02278	2.195	0.749
$I_{SZ,R}$, cm ⁴	0	-0.543	-0.152
$I_{Z,R}$, cm ⁴	0.534	0.171	0.0646
$I_{1,R}$, cm ⁵	0	1.408	0
$I_{2,R}$, cm ⁵	-0.0848	-0.3880	0
J_R , cm ⁴	0.01523	0.003580	0.003580
$J_{e,R}$, cm ⁴	0.5572	2.366	0.814
Γ_R , cm ⁶	0.01634	1.08	0.13185

TABLE II.- PROGRAM INPUT PARAMETERS - Concluded

(c) Analysis method 11

Shell and rings:

Young's modulus, E_1 and E_2 , GN/m ²	68.95
Poisson's ratio, μ	0.315
Mass density, ρ , kg/m ³	2.715

Shell:

Thickness, h_1 and h_2 , cm.	0.03175
s_0 , cm	8.799
ϵ_1 , cm	2.933
ϵ_2 , cm	5.866

Rings:

Parameter	Base	Small Z	Large Z
Juncture	2	7	12
$\hat{\epsilon}_1$, cm	0.6232	-1.2648	-1.2648
$\hat{\epsilon}_3$, cm	1.3335	0.8065	0.8065
ϕ , deg	-60	-60	-60
EI_1 , N-m ²	93.083	70.732	70.732
EI_3 , N-m ²	273.787	483.534	483.534
EI_{13} , N-m ²	156.494	-150.010	-150.010
EA, mN	5.1366	4.2470	4.2470
$E\Gamma_3$, mN-m ⁴	0.3025	6.359	6.359
GJ, N-m ²	4.154	0.9286	0.9286
z, cm	-0.03175	-0.03175	-0.03175
m_1 , g/m	0.523	0.503	0.503

TABLE III.- FREQUENCY RESULTS FOR FREE-RING STIFFENERS

n	Experiment	Analysis			Experiment	Analysis		
		Method 9	Method 10	Method 11		Method 9	Method 10	Method 11
Frequency, Hz, for m = 1					Frequency, Hz, for m = 2			
Large Z-ring								
0	----	0	0	0	----	0	0.34	0
1	----	0	.24	0	----	0	2.83	0
2	8.8	6.37	6.98	6.42	16.2	14.2	17.9	14.4
3	25.0	25.2	27.1	25.8	46.4	41.2	44.9	41.6
4	64.2	59.4	64.9	62.1	90.3	84.0	86.3	83.9
5	107.1	105.6	115.9	111.4	153.6	149.9	151.5	150.1
6	161.2	160.8	174.4	169.4	244.6	241.9	246.4	244.9
7	223.1	225.1	241.7	236.5	357.0	355.9	366.3	364.2
8	295.7	298.5	318.7	313.3	----	486.8	505.2	502.4
Small Z-ring								
0	----	0	0	0	----	0	1.01	0
1	----	0	.95	0	----	0	8.47	0
2	21.2	19.8	22.9	20.4	41.4	42.3	53.6	43.3
3	86.5	79.5	90.5	84.4	126.0	124.2	135.1	125.7
4	190.0	184.2	211.8	199.4	251.0	257.4	266.8	260.7
5	315.0	320.3	359.2	344.4	443.0	457.0	480.2	473.5
6	472.0	482.3	530.4	515.4	----	714.9	764.4	755.3
7	668.0	670.6	730.1	715.0	----	1016.0	1099.0	1088.0

TABLE IV.- FREQUENCY RESULTS FOR MODEL CONFIGURATIONS 1C, 1C̄, AND 1S

n	Configuration 1C̄		Configuration 1C				Configuration 1S	
	Experiment	Analysis methods 9, 10, and 11	Experiment	Analysis			Experiment	Analysis method 12
				Method 9	Method 10	Method 11		
Frequency, Hz, for m = 1								
0	----	537.3	----	519.7	515.2	513.1	----	---
1	----	129.5	----	107.9	100.6	95.9	50.1	44.4
2	50.8	58.5	43.8	46.7	46.2	42.0	27.9	31.8
3	{ 27.2 28.2 }	32.7	25.4	25.8	25.9	25.3	20.7	23.8
4	{ 19.8 21.2 }	23.0	19.6	19.5	19.5	19.8	18.7	19.5
5	{ 20.3 21.5 }	22.4	21.0	21.4	21.4	21.6	22.0	20.9
6	{ 26.5 27.4 }	27.1	26.7	26.9	26.9	27.0	26.9	26.0
7	{ 33.1 33.7 }	33.6	{ 33.1 33.7 }	33.6	33.6	33.6	{ 33.1 33.7 }	32.4
8	{ 40.6 41.3 }	41.0	{ 40.6 41.3 }	41.0	41.0	41.0	{ 40.6 41.3 }	39.5
9	{ 47.9 49.3 }	49.2	{ 47.9 49.3 }	49.2	49.2	49.2	{ 47.9 49.3 }	47.4
10	{ 57.8 58.5 }	58.1	{ 51.8 58.5 }	58.1	58.1	58.1	{ 57.8 58.5 }	56.1
11	{ 67.0 68.6 }	67.9	{ 67.0 68.6 }	67.9	67.9	67.9	{ 67.0 68.6 }	65.4
12	{ 78.6 79.2 }	78.4	{ 78.6 79.2 }	78.4	78.4	78.4	{ 78.6 79.2 }	75.6
13	{ 89.3 90.6 }	89.9	{ 89.3 90.6 }	89.9	89.8	89.9	{ 89.3 90.6 }	86.7
14	{ 101.4 102.0 }	102.2	{ 101.4 102.0 }	102.2	102.2	102.2	{ 101.4 102.0 }	98.5
15	{ 113.5 115.0 }	115.3	{ 113.5 115.0 }	115.3	115.3	115.3	{ 113.5 115.0 }	---

TABLE V.- RESULTS FOR MODEL CONFIGURATIONS 2C AND 2S

n	Configuration 2C								Configuration 2S
	Experiment	Analysis			Experiment	Analysis			Experiment
		Method 9	Method 10	Method 11		Method 9	Method 10	Method 11	
Frequency, Hz, for m = 1					Frequency, Hz, for m = 2				Frequency, Hz, for m = 1
0	----	411.4	412.5	402.3	----	645.0	625.8	628.5	----
1	----	85.7	80.1	76.5	----	575.7	577.2	556.2	41.7
2	38.2	38.8	38.4	34.9	----	485.7	479.6	466.9	25.1
3	42.5	46.2	42.4	40.9	309.1	313.2	314.9	315.1	40.5
4	80.5	87.5	75.8	79.5	{ 208.9 211.2 }	209.0	214.1	215.2	{ 69.5 70.0 }
5	123.0	127.5	115.3	125.8	{ 178.4 179.0 }	181.6	177.8	181.5	115.0
6	116.6	118.5	116.8	119.0	242.1	251.0	231.5	260.9	116.6
7	115.3	115.0	114.9	114.6	276.5	290.0	279.9	291.1	115.3
8	116.9	118.3	118.6	117.3	264.8	274.4	273.0	274.2	116.9
9	123.2	124.6	125.0	123.4	----	267.9	267.9	264.7	123.2
10	130.7	132.9	133.3	131.4	{ 258.1 261.3 }	267.4	267.8	264.0	130.7
11	139.6	142.8	143.2	141.1	265.9	271.1	271.5	267.5	139.6
12	150.4	154.2	154.6	152.3	----	278.0	278.4	274.2	150.4
13	162.3	166.9	167.3	164.7	----	287.7	288.0	283.7	162.3
14	175.5	181.0	181.4	178.5	{ 290.2 295.9 }	299.8	300.1	295.6	175.5
15	187.2	196.3	196.7	193.5	----	314.0	314.3	309.5	187.2
16	201.9	212.8	213.3	209.7	----	330.1	330.5	325.4	201.9
17	221.4	230.5	231.0	227.1	----	348.1	348.5	343.1	221.4
18	243.0	249.3	249.9	245.6	----	367.8	368.3	362.4	243.0

TABLE VI.- RESULTS FOR MODEL CONFIGURATION 3C

n	Experiment	Analysis			Experiment	Analysis		
		Method 9	Method 10	Method 11		Method 9	Method 10	Method 11
		Frequency, Hz, for m = 1				Frequency, Hz, for m = 2		
0	----	406.8	406.7	396.4	----	625.5	610.4	607.5
1	70.4	83.8	77.3	74.1	----	563.9	562.6	542.6
2	40.3	39.2	50.8	40.2	----	437.4	441.6	423.3
3	60.1	54.7	80.5	67.6	286.0	272.4	357.8	305.2
4	102.0	106.6	102.8	103.8	399.0	231.7	382.7	329.8
5	159.0	170.3	149.4	163.4	330.0	324.3	384.1	380.4
6	235.6	251.4	222.2	257.0	307.0	342.4	354.9	345.2
7	263.5	284.8	270.7	286.9	307.0	338.7	334.1	324.8
8	245.8	253.7	256.6	253.3	{ 316.0 326.0 }	{ 334.9	336.8	322.6
9	{ 211.5 216.0 }	227.2	235.3	226.8	342.0	346.6	354.8	336.1
10	200.0	207.9	218.0	208.0	359.0	366.9	381.4	358.8
11	183.2	195.8	206.1	196.1	399.0	389.2	413.4	387.5
12	----	190.4	199.7	190.4	438.0	398.1	426.8	405.1
13	178.0	190.8	198.5	190.3	----	391.0	412.6	391.1
14	----	196.2	202.2	195.0	----	383.5	402.2	381.3
15	201.0	205.6	210.1	203.7	----	379.7	396.4	376.5
16	{ 211.0 217.0 }	218.4	221.5	215.8	----	380.3	395.2	376.6
17	226.0	233.7	235.8	230.6	----	385.3	398.6	381.3
18	246.0	251.2	252.6	247.5	----	394.6	406.4	390.3
19	264.0	270.5	271.3	266.2	400.0	407.9	418.1	403.3
20	286.0	291.2	291.7	286.5	----	425.0	433.5	419.8
21	{ 309.0 315.0 }	----	313.6	----	----	----	452.1	----
22	{ 327.0 330.0 343.0 }	----	336.7	----	----	----	473.6	----
23	358.0	----	----	----	----	----	----	----

**TABLE VII.- FREQUENCY RESULTS OF PARAMETRIC STUDY
OF ATTACHMENT GEOMETRY**

(a) Method 9

n	Experiment	Analysis			Experiment	Analysis		
		Type 1	Type 2	Type 3		Type 1	Type 2	Type 3
		Frequency, Hz, for m = 1				Frequency, Hz, for m = 2		
0	----	406.8	407.7	403.7	----	625.5	630.7	622.8
1	70.4	83.8	83.9	77.0	----	563.9	564.6	561.6
2	40.3	39.2	46.5	45.6	----	437.4	440.6	435.4
3	60.1	54.7	76.2	76.3	286.0	272.4	321.6	322.2
4	102.0	106.6	111.4	111.4	399.0	231.7	357.3	360.9
5	159.0	170.3	170.3	170.3	330.0	324.3	397.5	399.7
6	235.6	251.4	251.7	251.7	307.0	342.4	346.6	348.2
7	263.5	284.8	389.9	290.1	307.0	338.7	341.2	344.2
8	245.8	253.7	261.3	261.4	316.0 326.0	334.9	338.3	339.7
9	211.5 216.0	227.2	236.3	236.3	342.0	346.6	352.9	353.5

	Model component			
	Shell	Base ring	Small Z-ring	Large Z-ring
Type 1: Boundary conditions* Attachments**	f-f ---	c-f (1-4)	f-f (1-3)	f-f (1-4)
Type 2: Boundary conditions* Attachments**	f-f ---	c-f (1-4)	f-f (1-4)	f-f (1-4)
Type 3: Boundary conditions* Attachments**	c-f ---	f-f (1-4)	f-f (1-4)	f-f (1-4)

*First designation is for component small diameter; second designation is for component large diameter; f indicates free; c indicates clamped.

**First digit indicates number of attachment circumferences per shell-ring interface; second digit indicates number of compatibility equations per attachment circumference; 3 indicates three displacement compatibility equations; 4 indicates three displacement and one rotation (about the circumference) compatibility equations.

TABLE VII. - FREQUENCY RESULTS OF PARAMETRIC STUDY
OF ATTACHMENT GEOMETRY - Concluded

(b) Method 11*

n	Experiment	Analysis		Experiment	Analysis	
		Attached at A	Attached at B		Attached at A	Attached at B
Frequency, Hz						
0	----	396.4	402.8	----	607.5	622.9
1	70.4	74.1	74.4	----	542.6	560.9
2	40.3	40.2	38.2	----	432.3	423.4
3	60.1	67.6	62.0	286.0	305.2	280.8
4	102.0	103.8	106.8	399.0	329.8	275.1
5	159.0	163.4	168.7	330.0	380.4	333.1
6	235.6	257.0	250.2	307.0	345.2	330.6
7	263.5	286.9	276.4	307.0	324.8	317.6
8	245.8	253.3	249.3	{ 316.0 326.0 }	322.6	322.3
9	{ 211.5 216.0 }	226.8	224.2	342.0	336.1	338.9

*Three displacements and the rotation of the ring are constrained to be equal to the shell displacements and rotation at the attachment circumference.

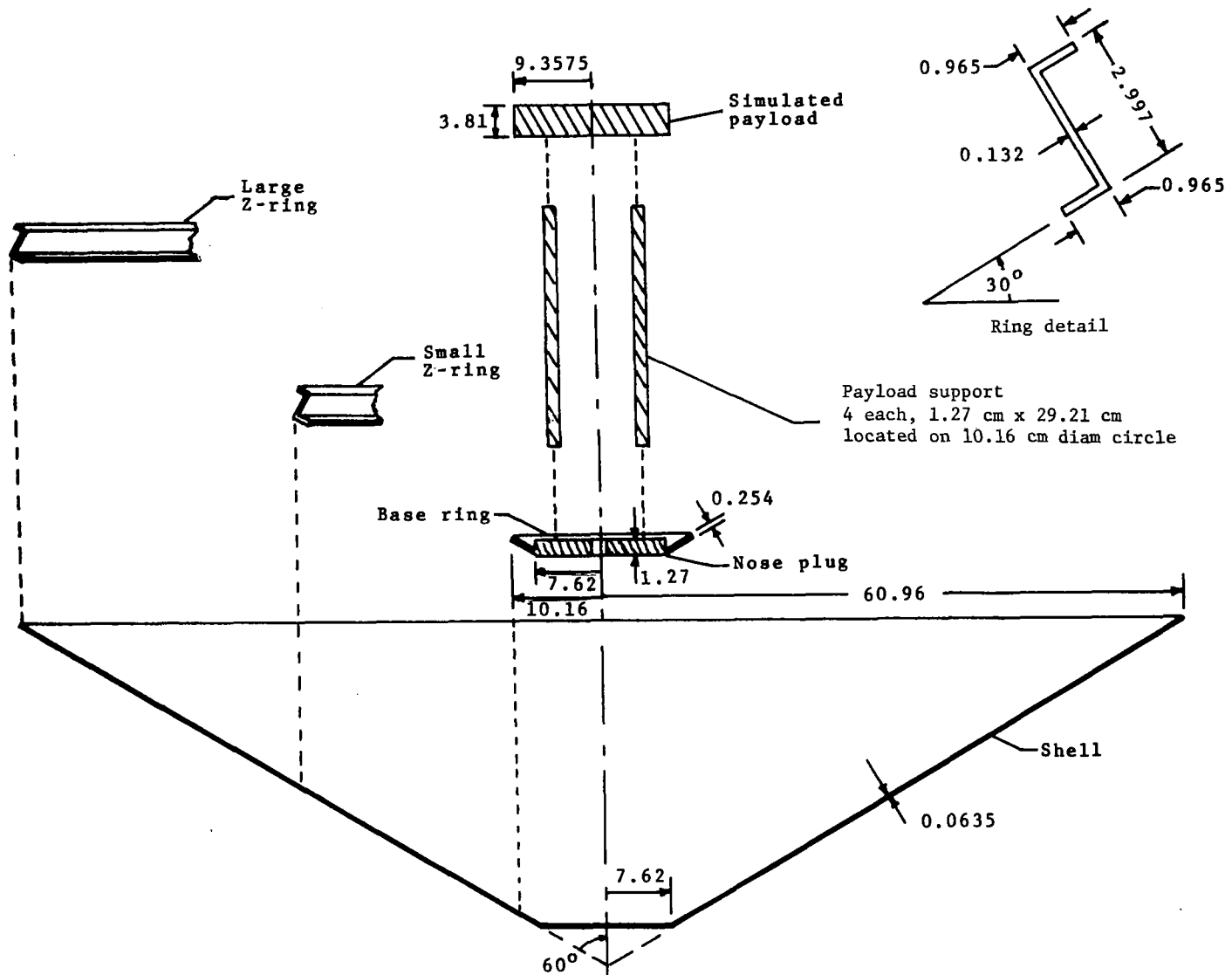


Figure 1.- Exploded schematic view of the various model components in their relative positions.
Linear dimensions are in centimeters.

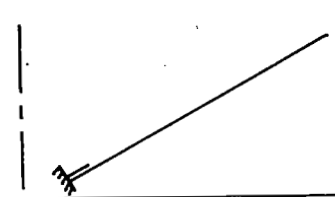
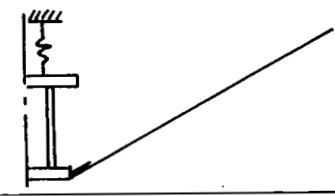
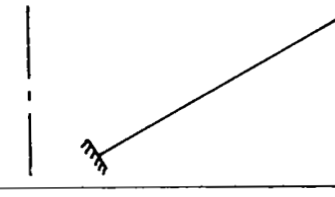
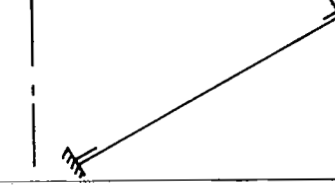
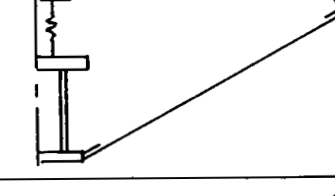
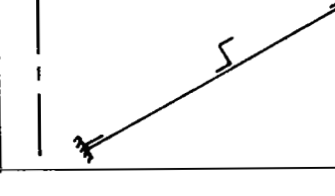
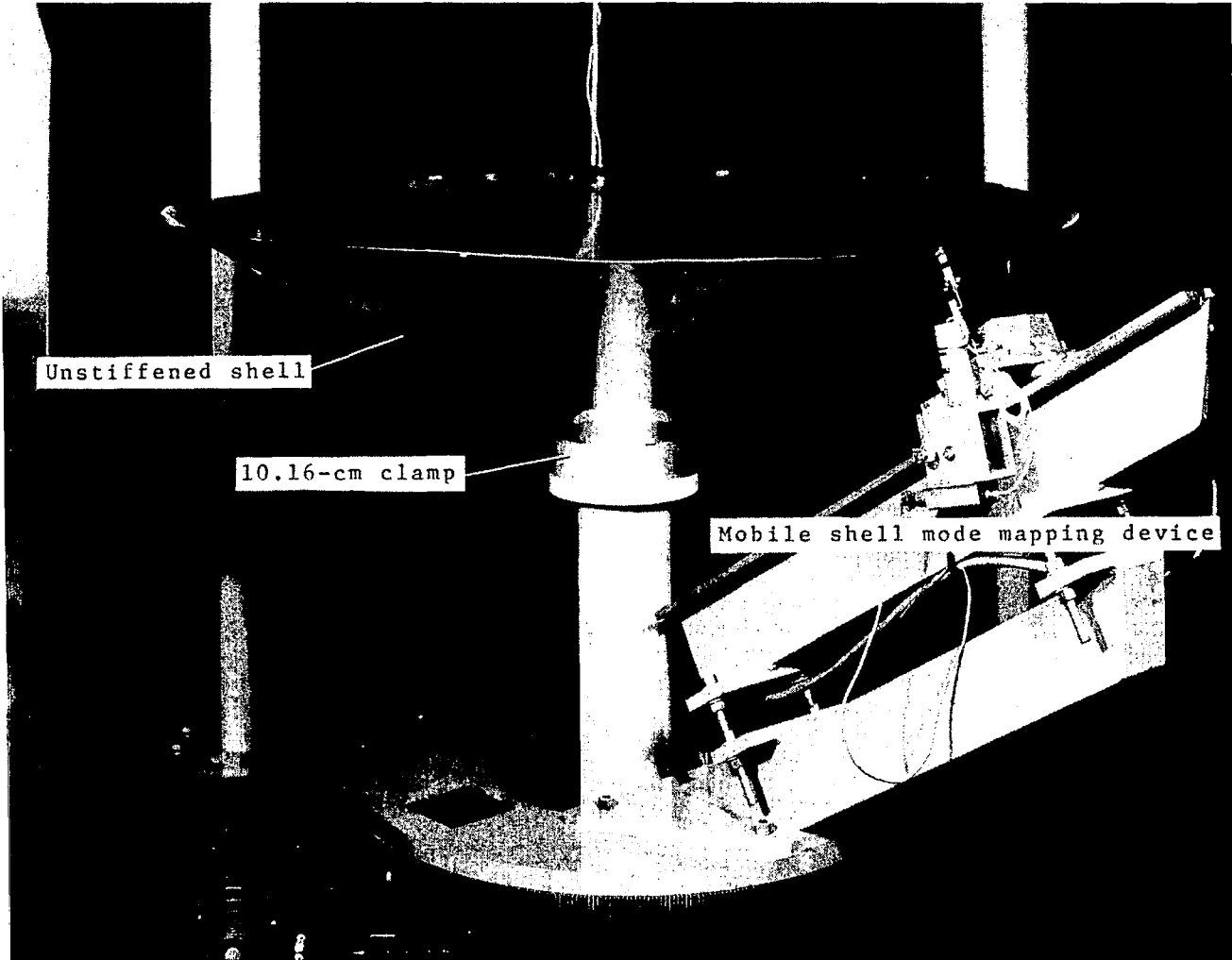
Model configuration	Component					Schematic representation
	Shell	Base ring	Small Z-ring	Large Z-ring	Simulated payload	
1C	X	X				
1S	X	X			X	
1C̄	X					
2C	X	X		X		
2S	X	X		X	X	
3C	X	X	X	X		

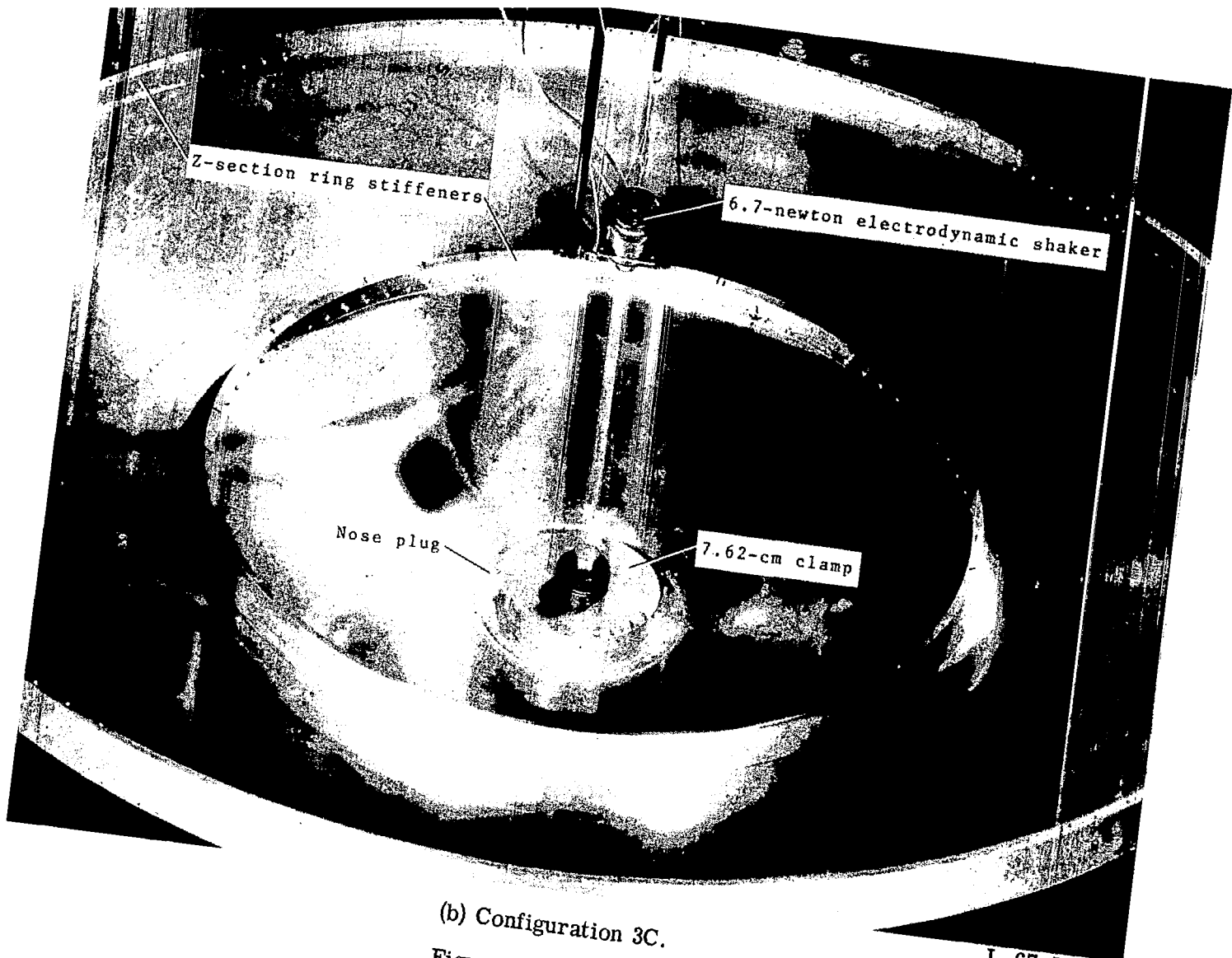
Figure 2.- Model configuration designation and schematic representation.



(a) Configuration 1C.

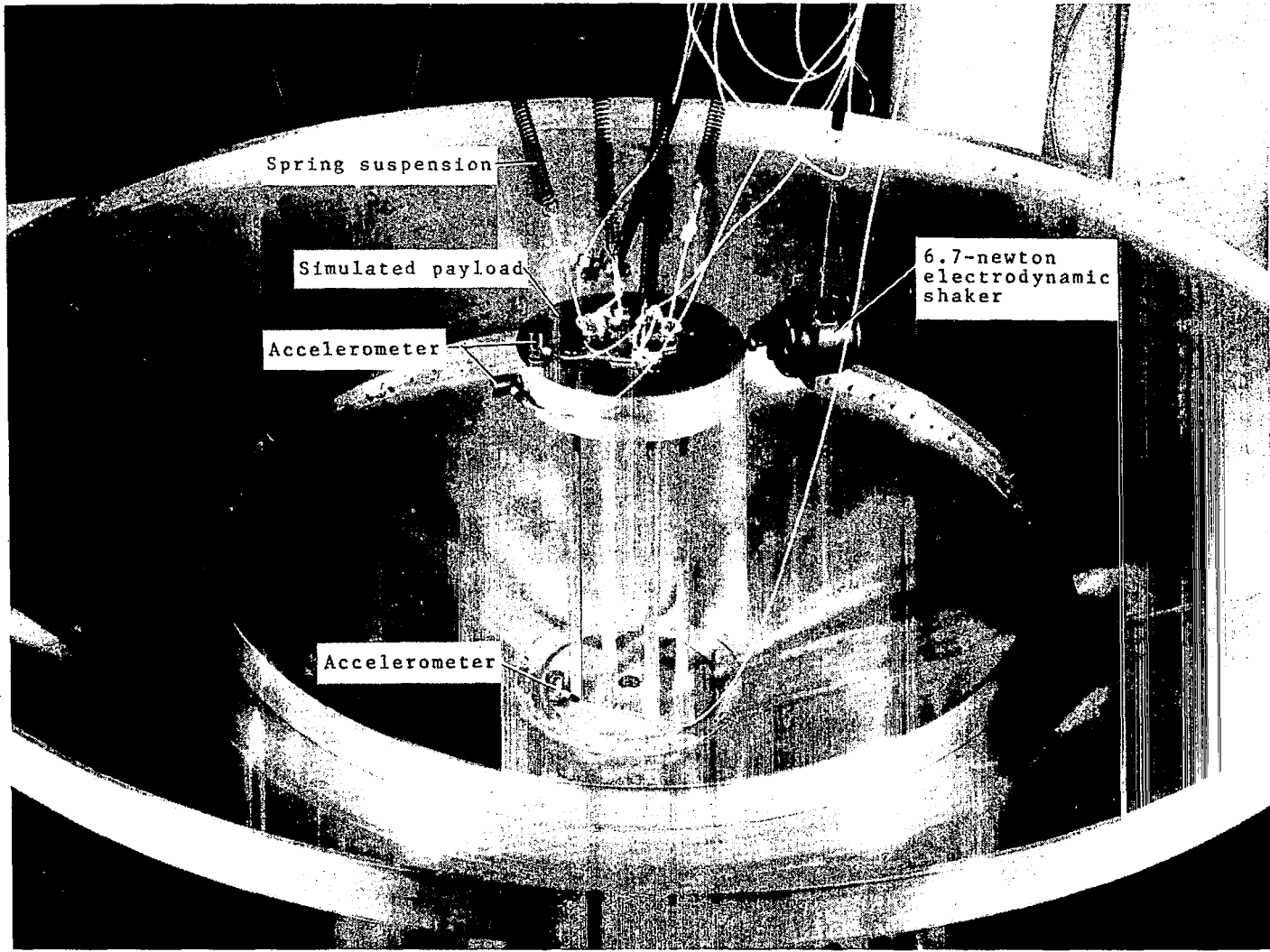
L-66-6185.1

Figure 3.- Test setup.



(b) Configuration 3C.
Figure 3.- Continued.

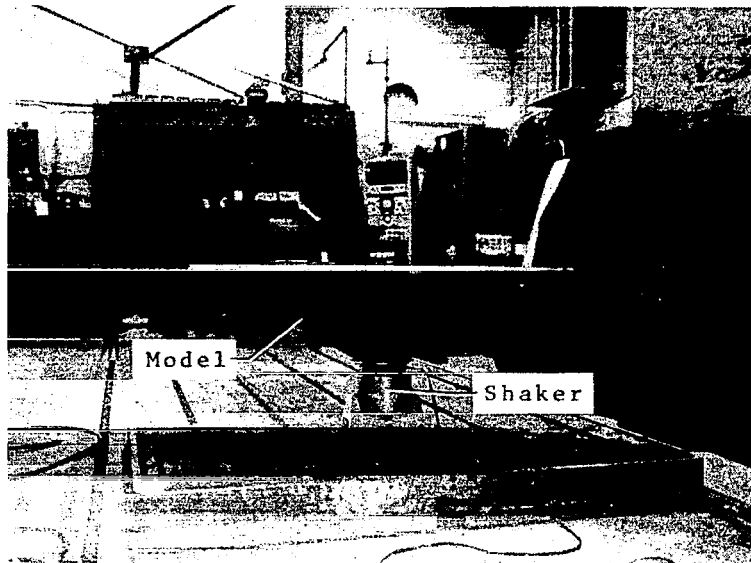
L-67-7542.1



L-67-7544.1

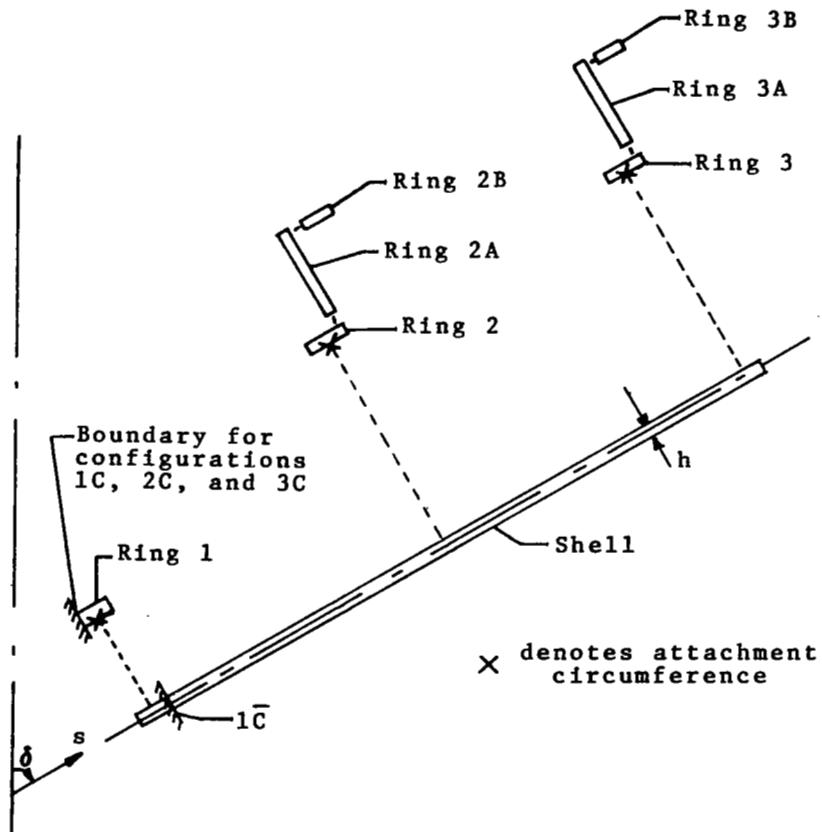
(c) Suspended tests.

Figure 3.- Continued.

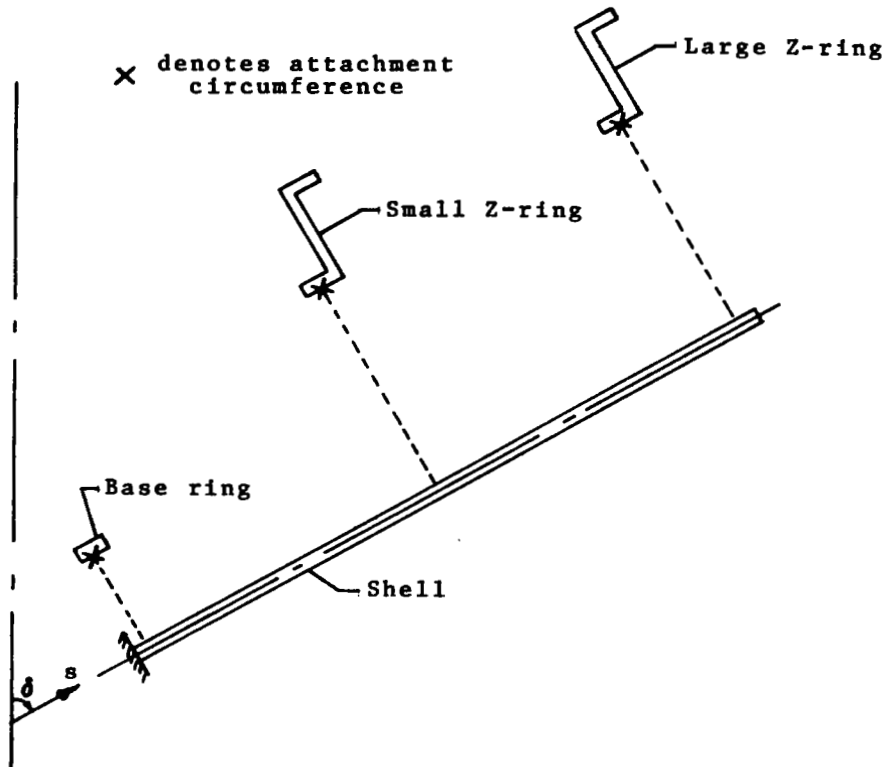


(d) Axisymmetric excitation.

Figure 3.- Concluded.

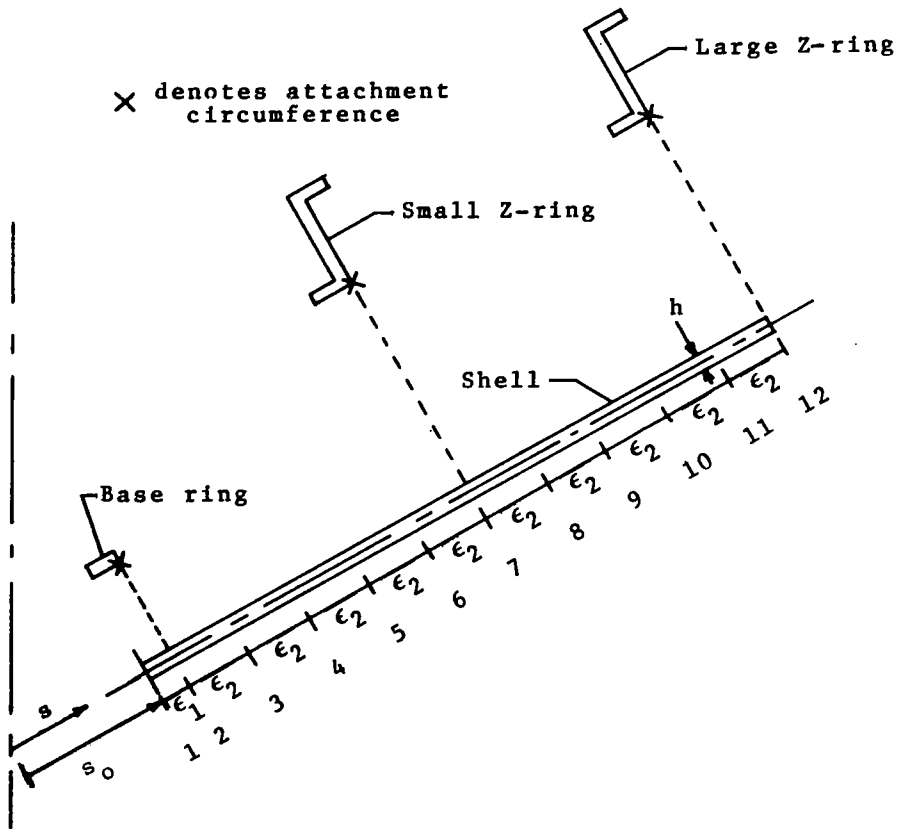


(a) Method 9. Ring designations are for table II(a).
 Figure 4.- Geometrical and idealization parameters.



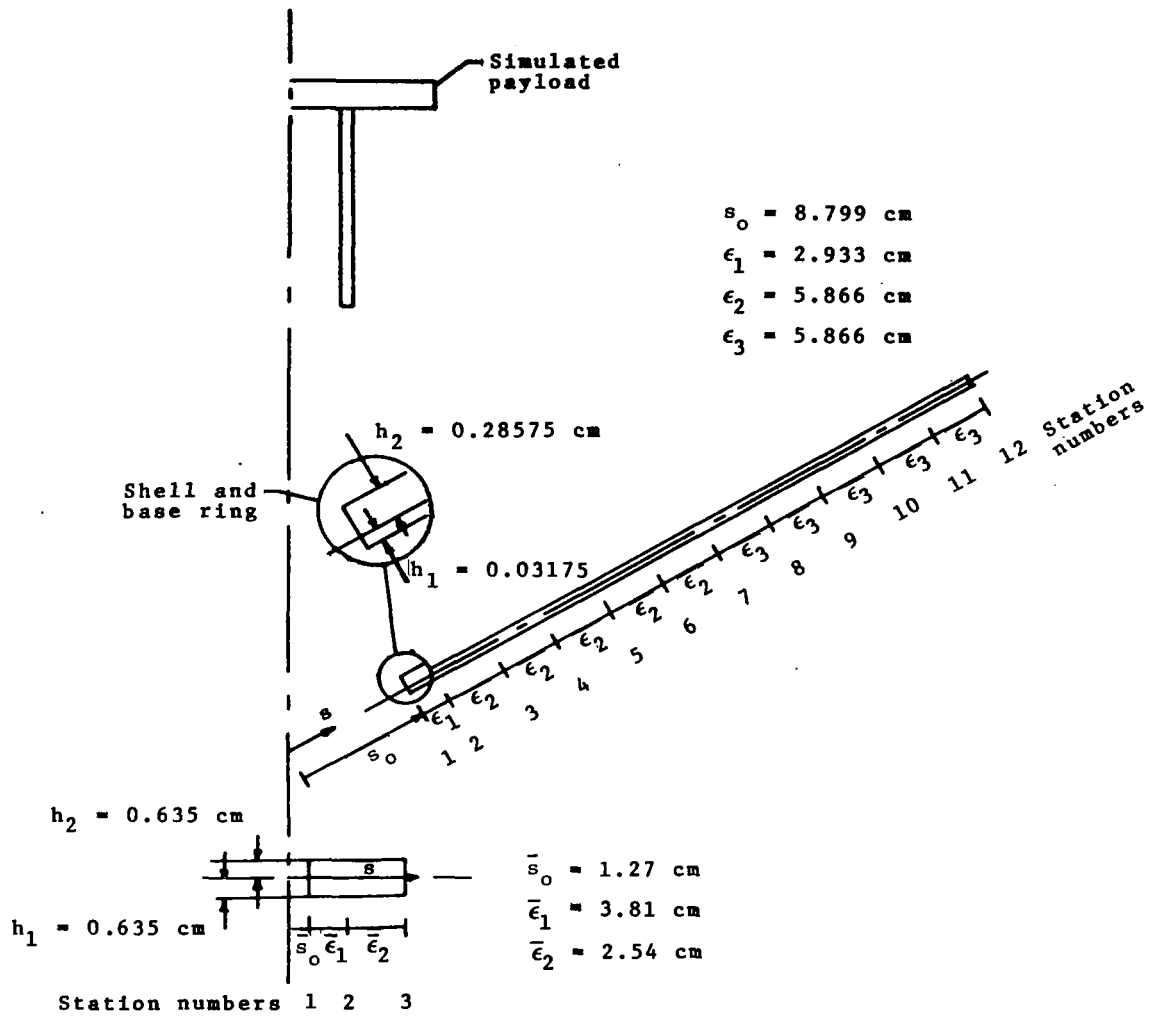
(b) Method 10.

Figure 4.- Continued.



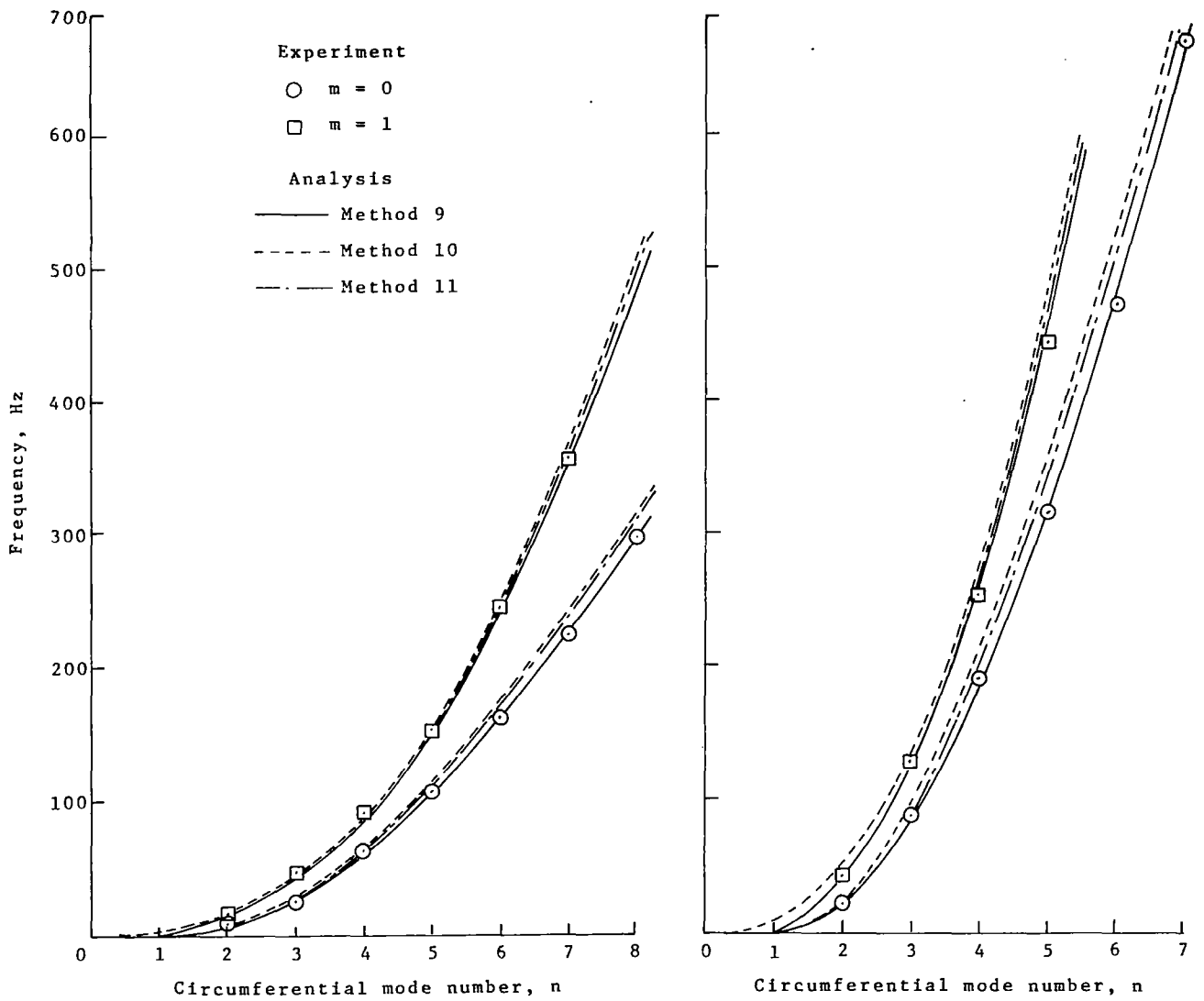
(c) Method 11.

Figure 4.- Continued.



(d) Method 12.

Figure 4.- Concluded.



(a) Large Z-ring.

(b) Small Z-ring.

Figure 5.- Frequency results for free rings.

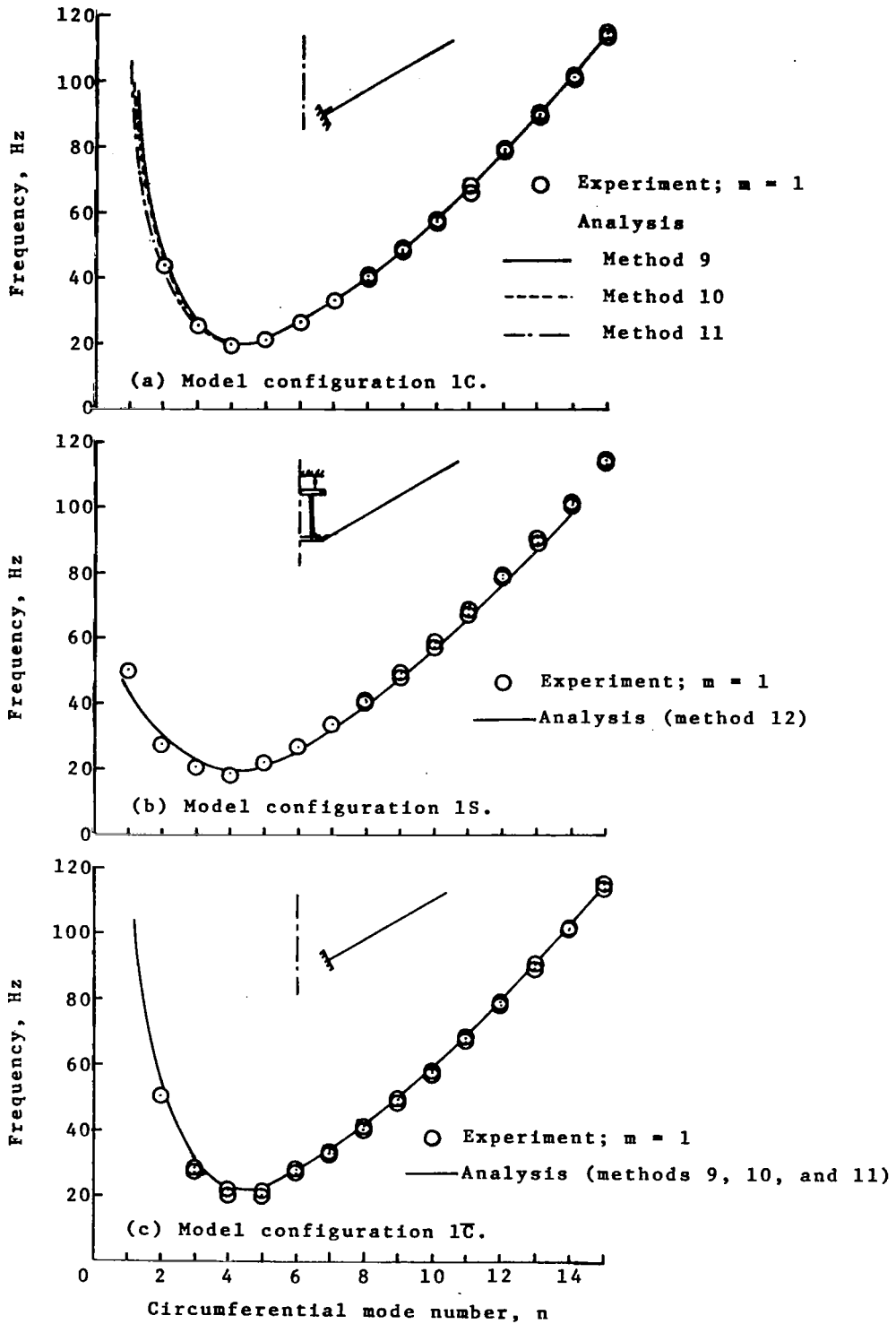
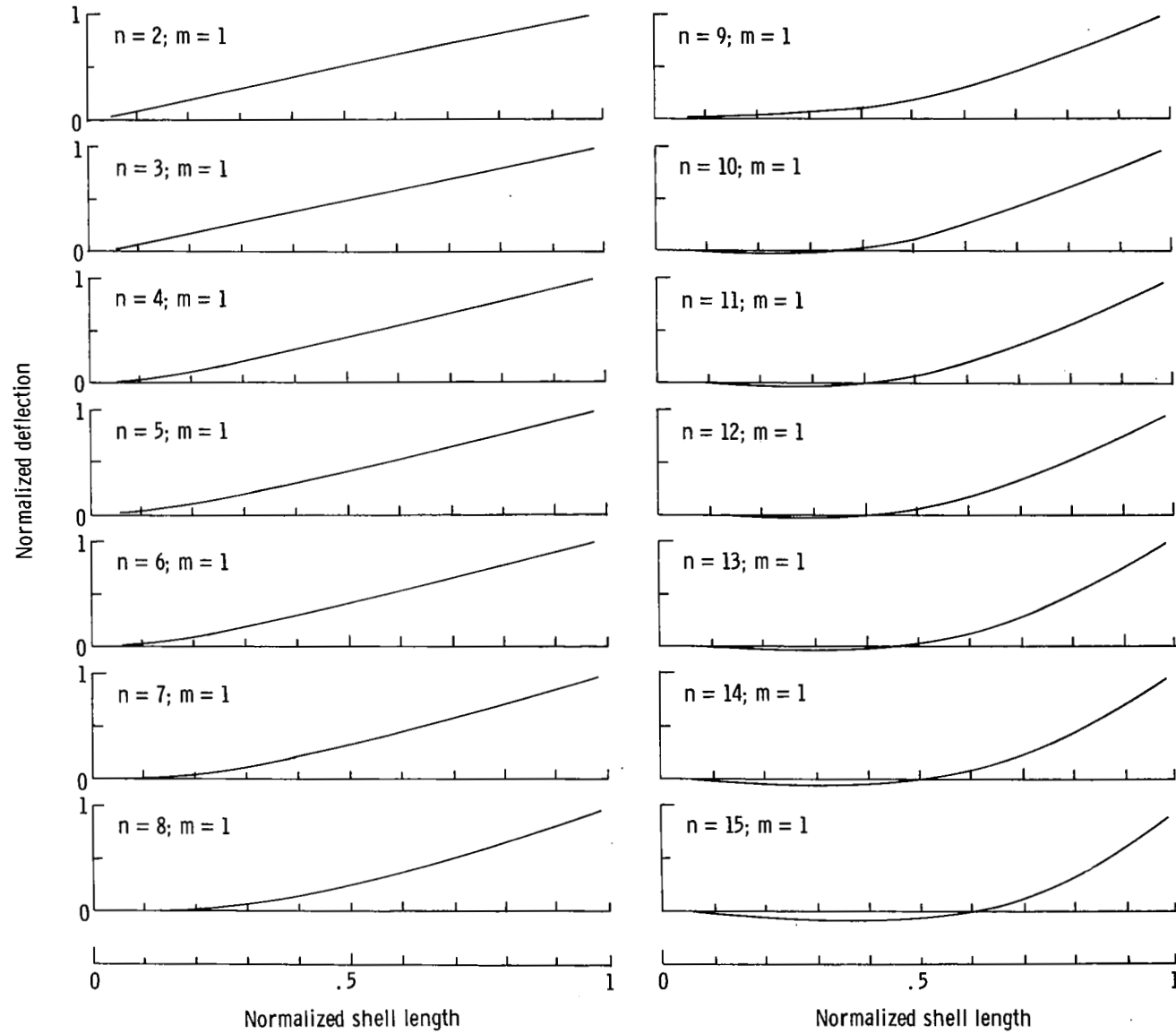
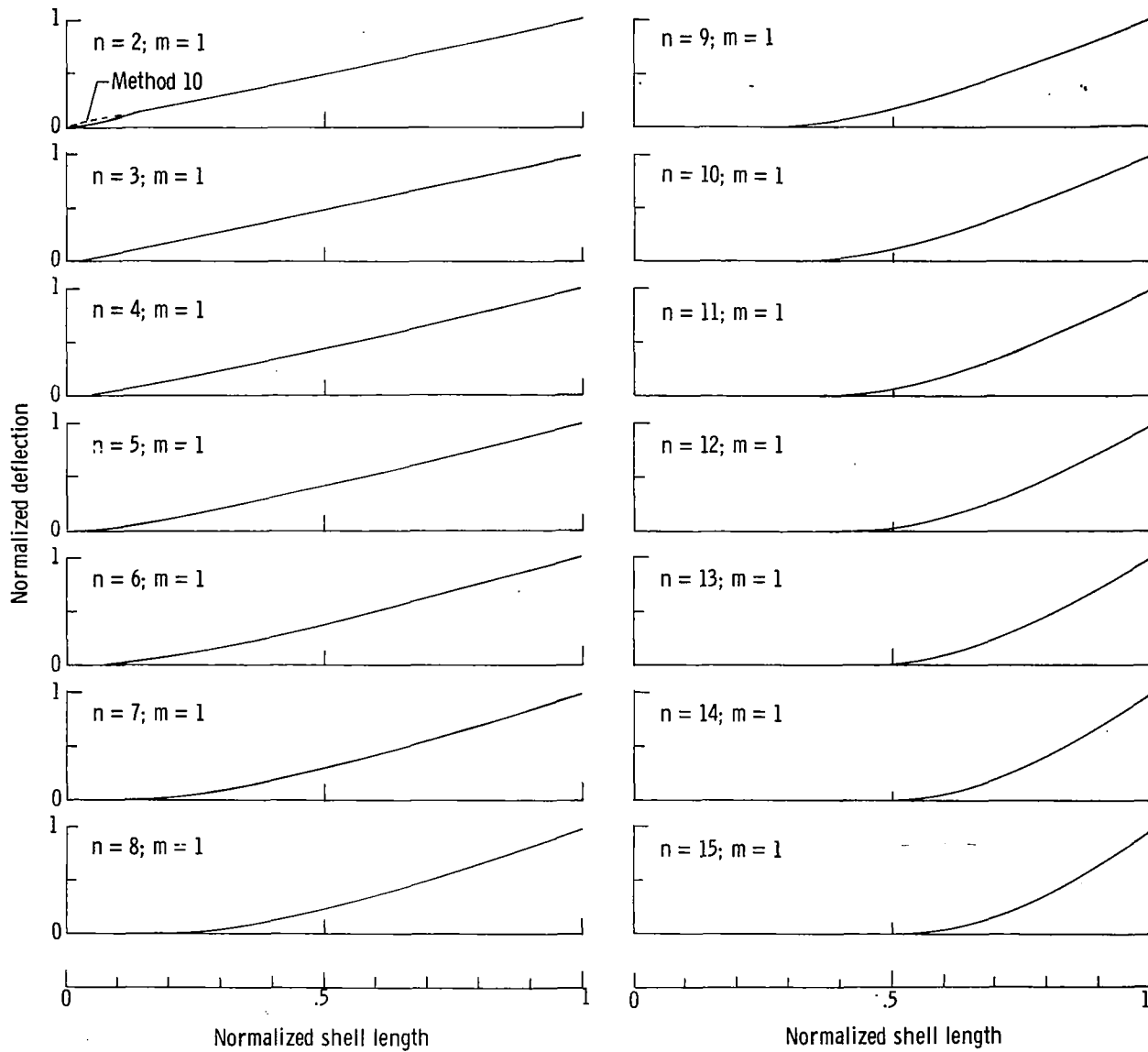


Figure 6.- Frequency results for model configurations 1C, 1S, and $\overline{1C}$.



(a) Experimental mode shapes.

Figure 7.- Mode shapes for model configuration 1C.



(b) Analytical mode shapes obtained by methods 9, 10, and 11.

Figure 7.- Concluded.

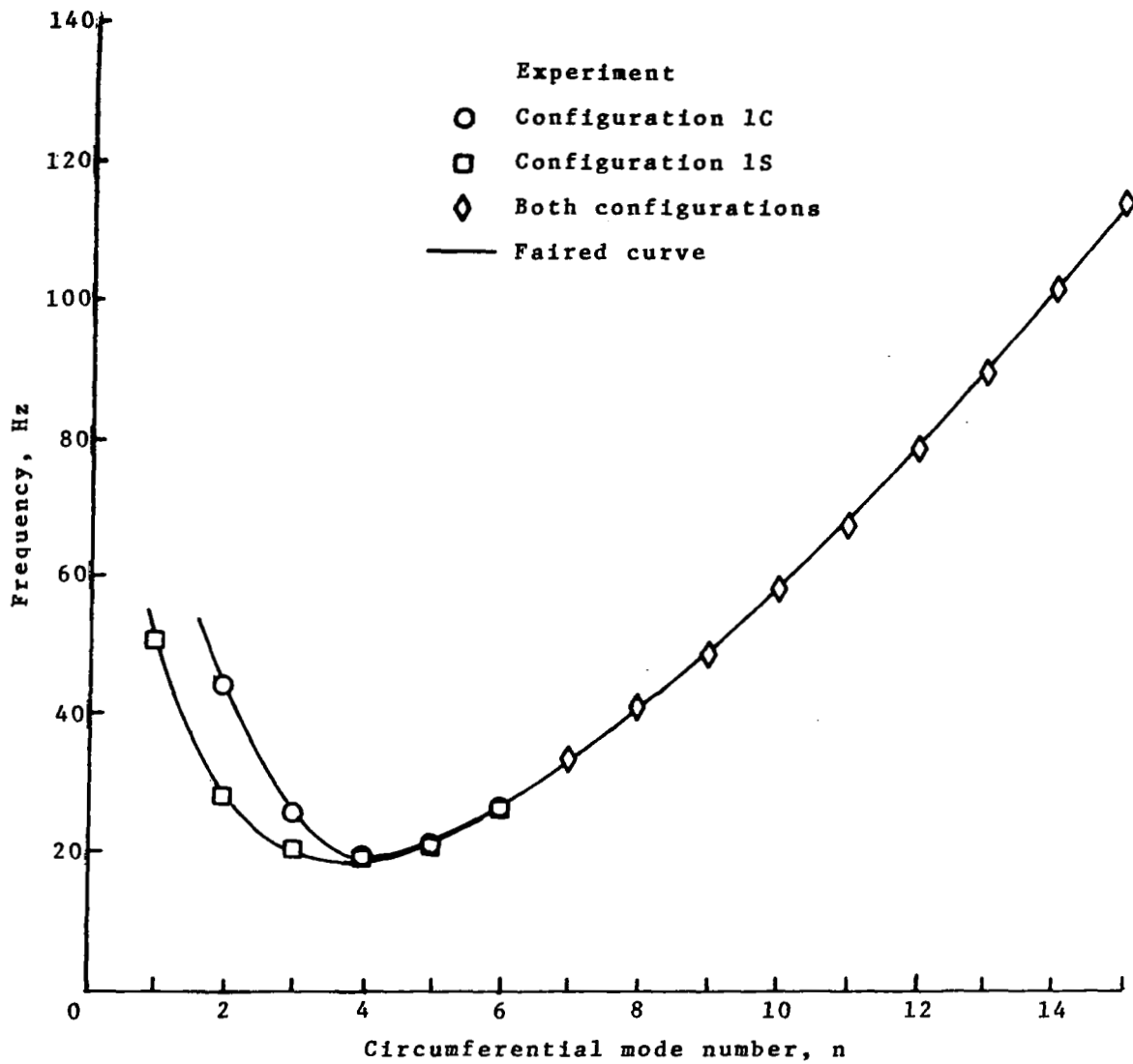


Figure 8.- Experimental frequency comparisons for model configurations 1C and 1S.

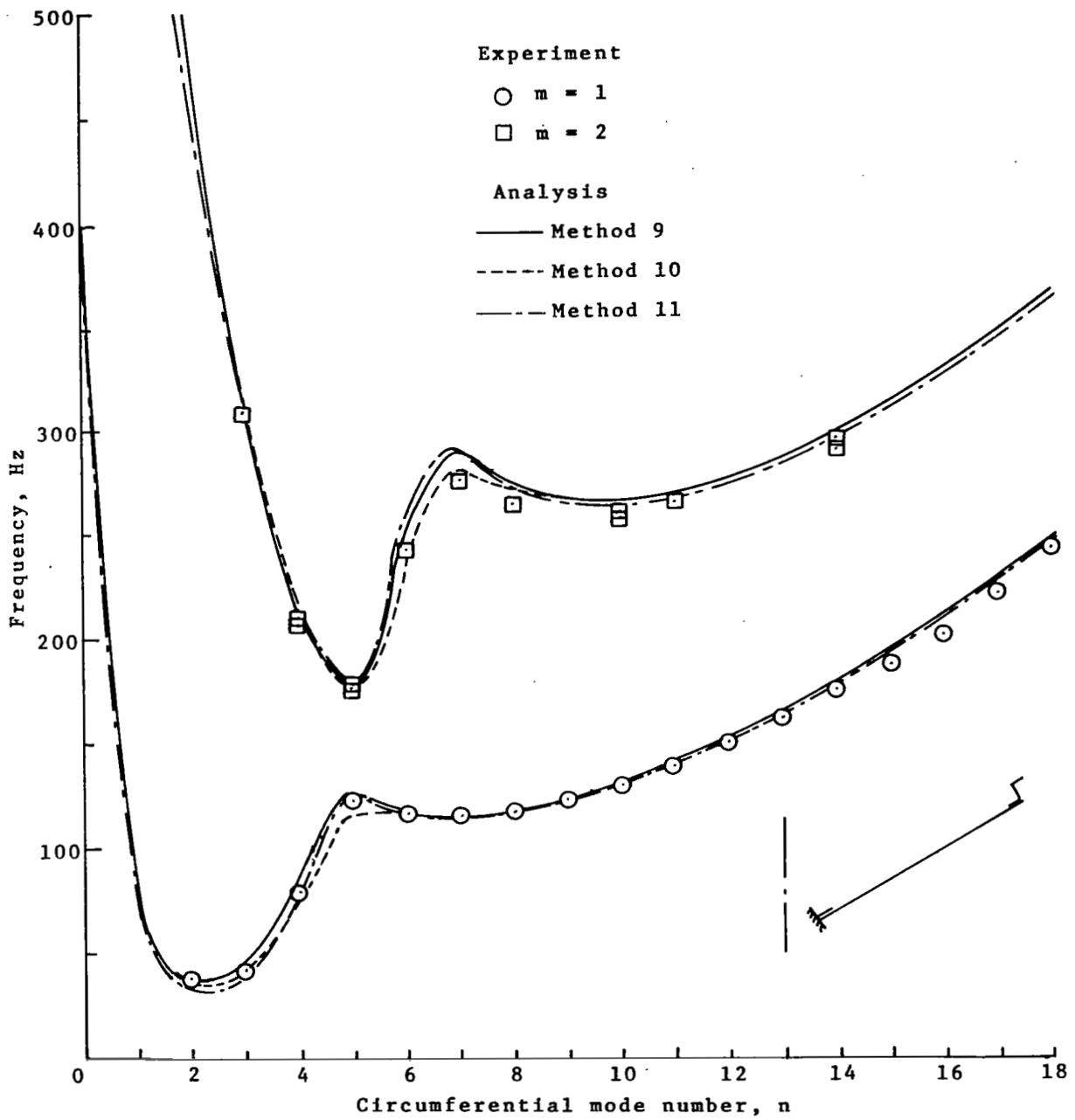
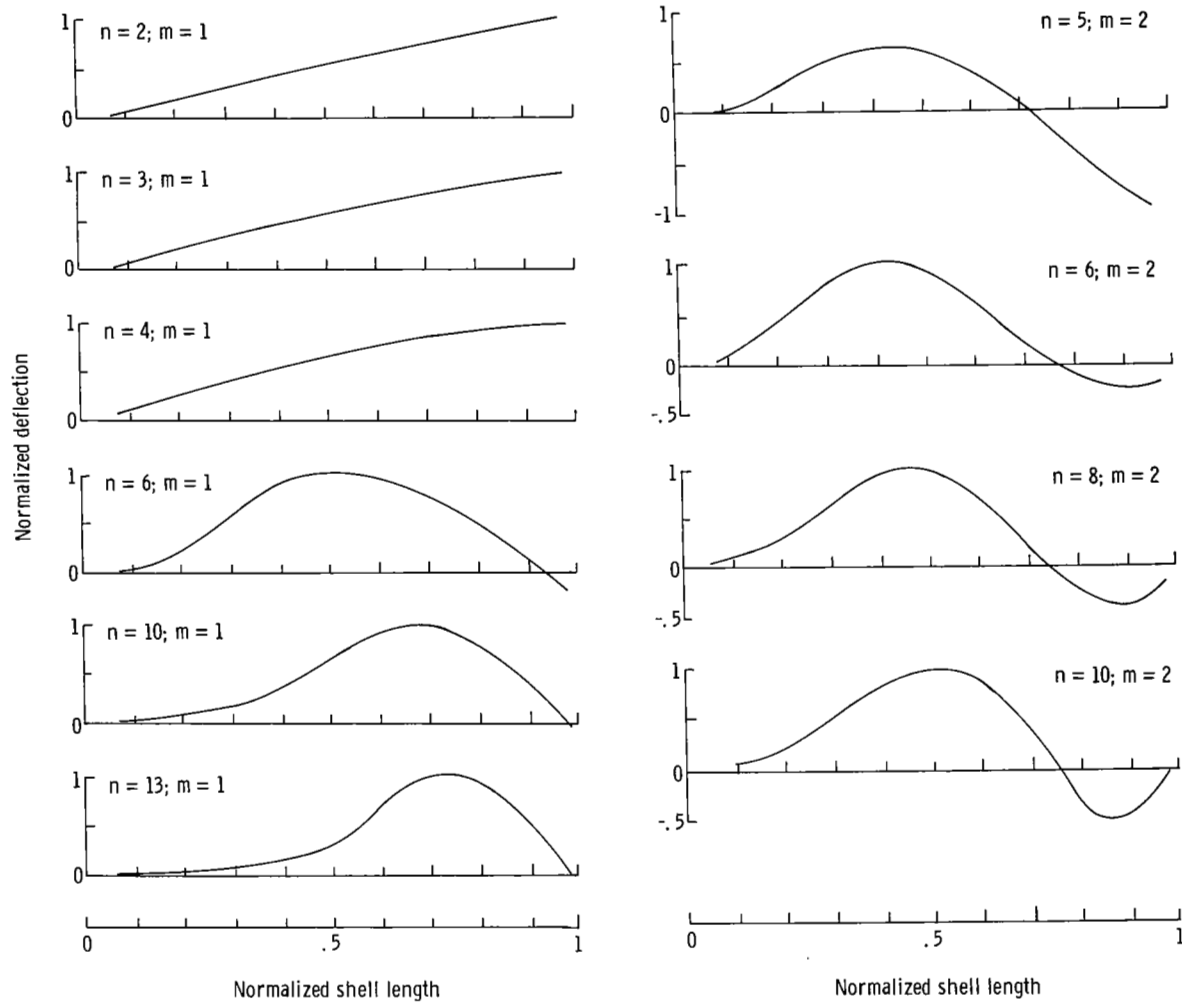
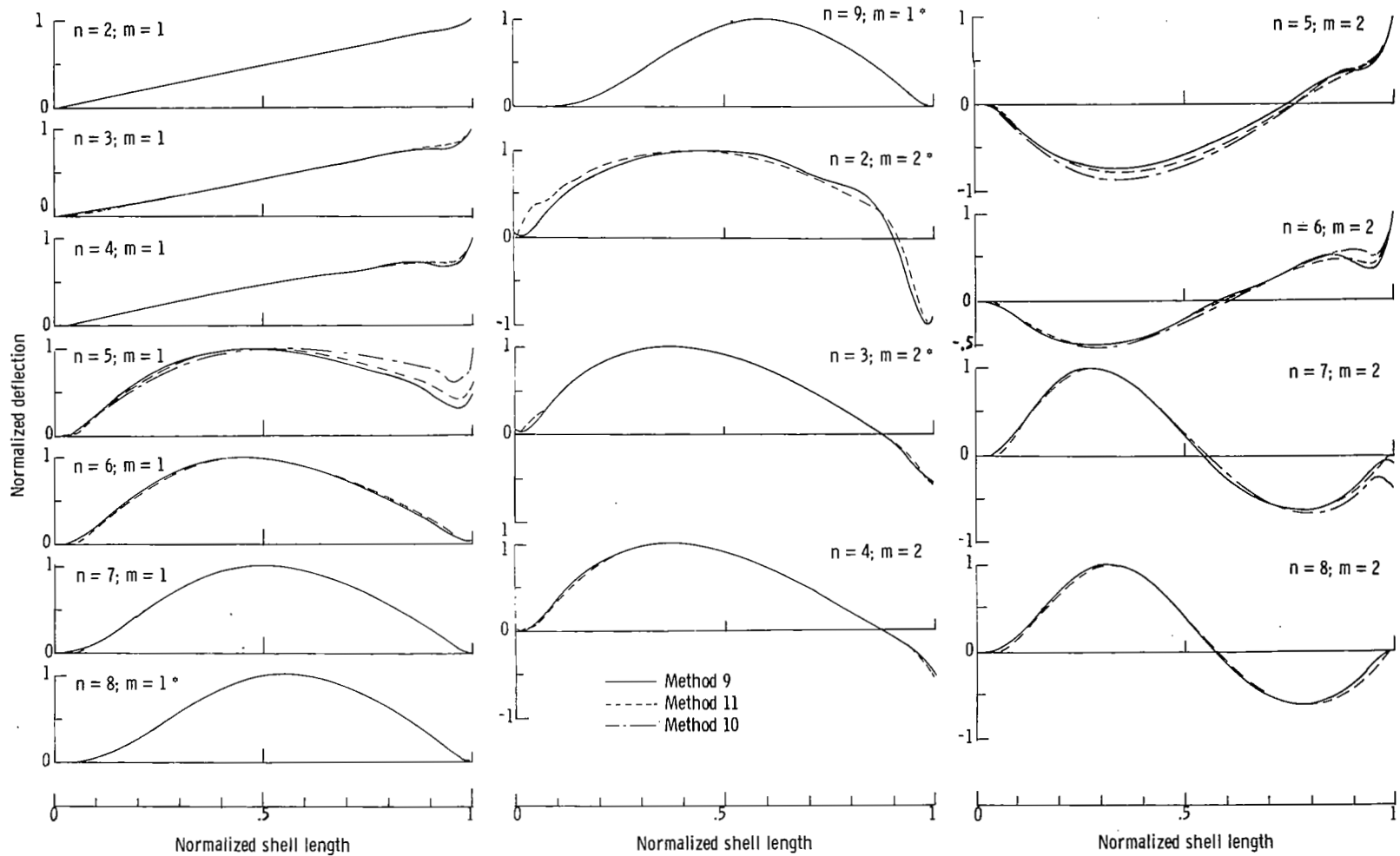


Figure 9.- Comparison of frequency results for model configuration 2C.



(a) Experimental mode shapes.

Figure 10.- Normalized experimental and analytical mode shapes for model configuration 2C.



(b) Analytical mode shapes obtained by methods 9, 10, and 11. Asterisk denotes that mode shapes for method 10 not available.

Figure 10.- Concluded.

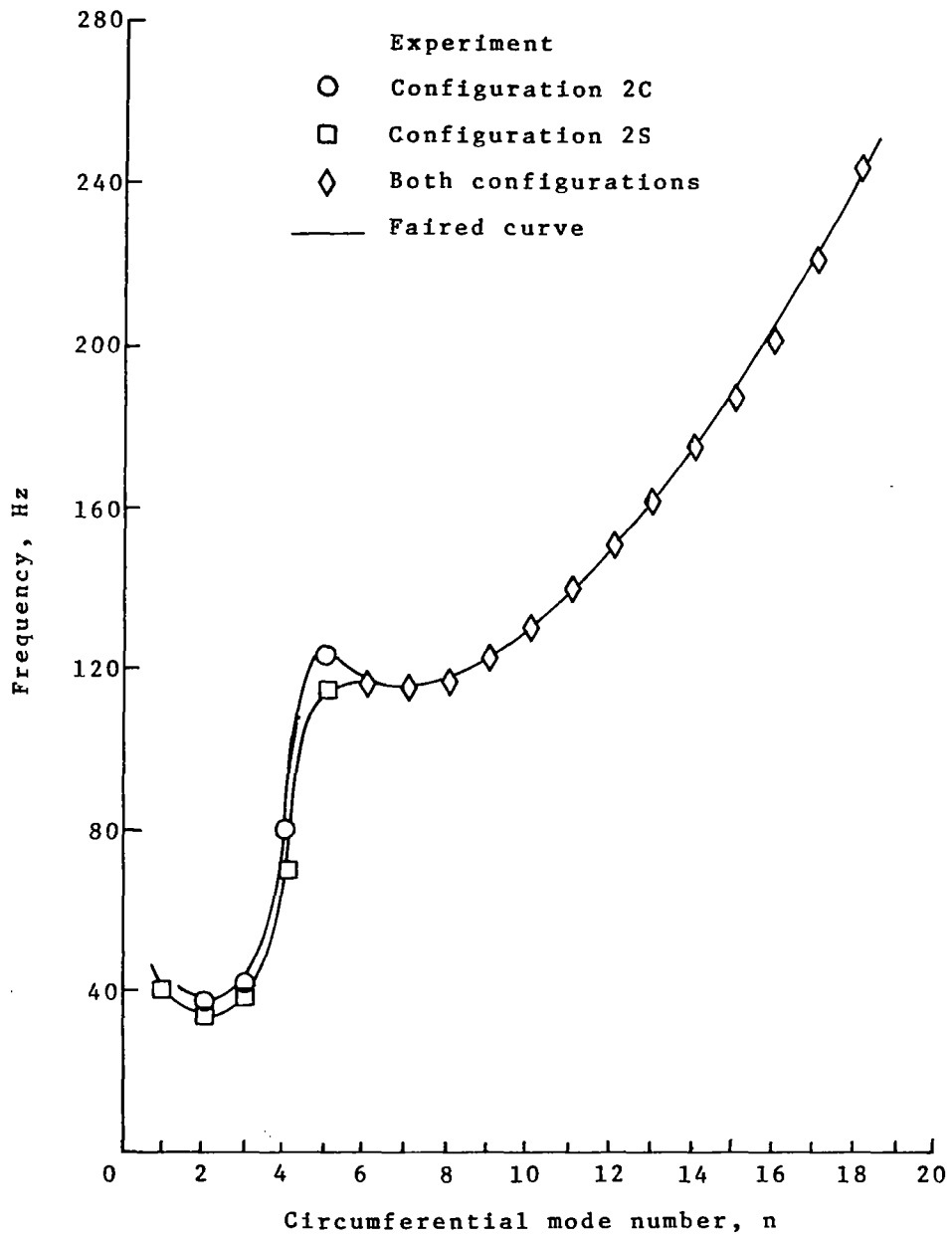


Figure 11.- Experimental comparisons for model configurations 2C and 2S.

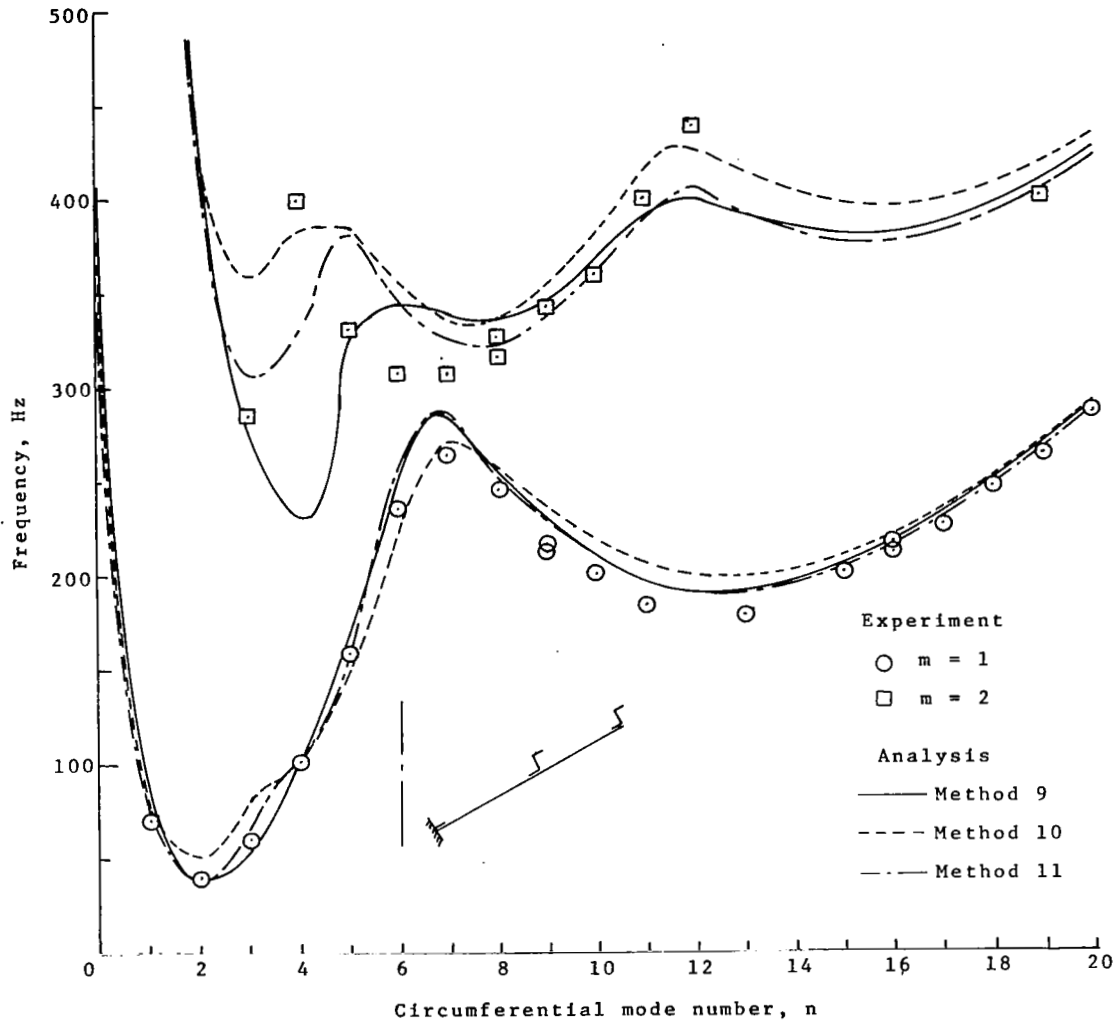
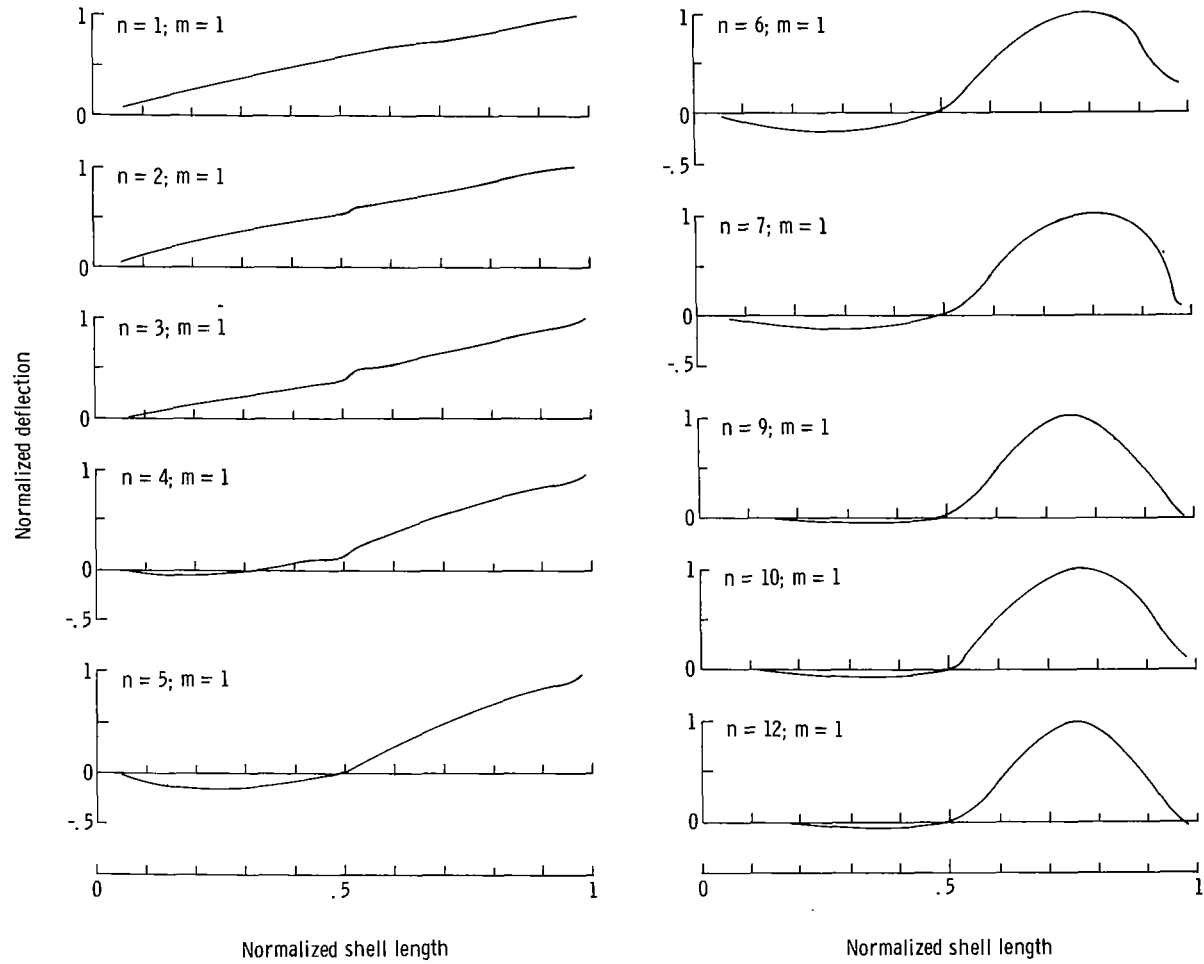
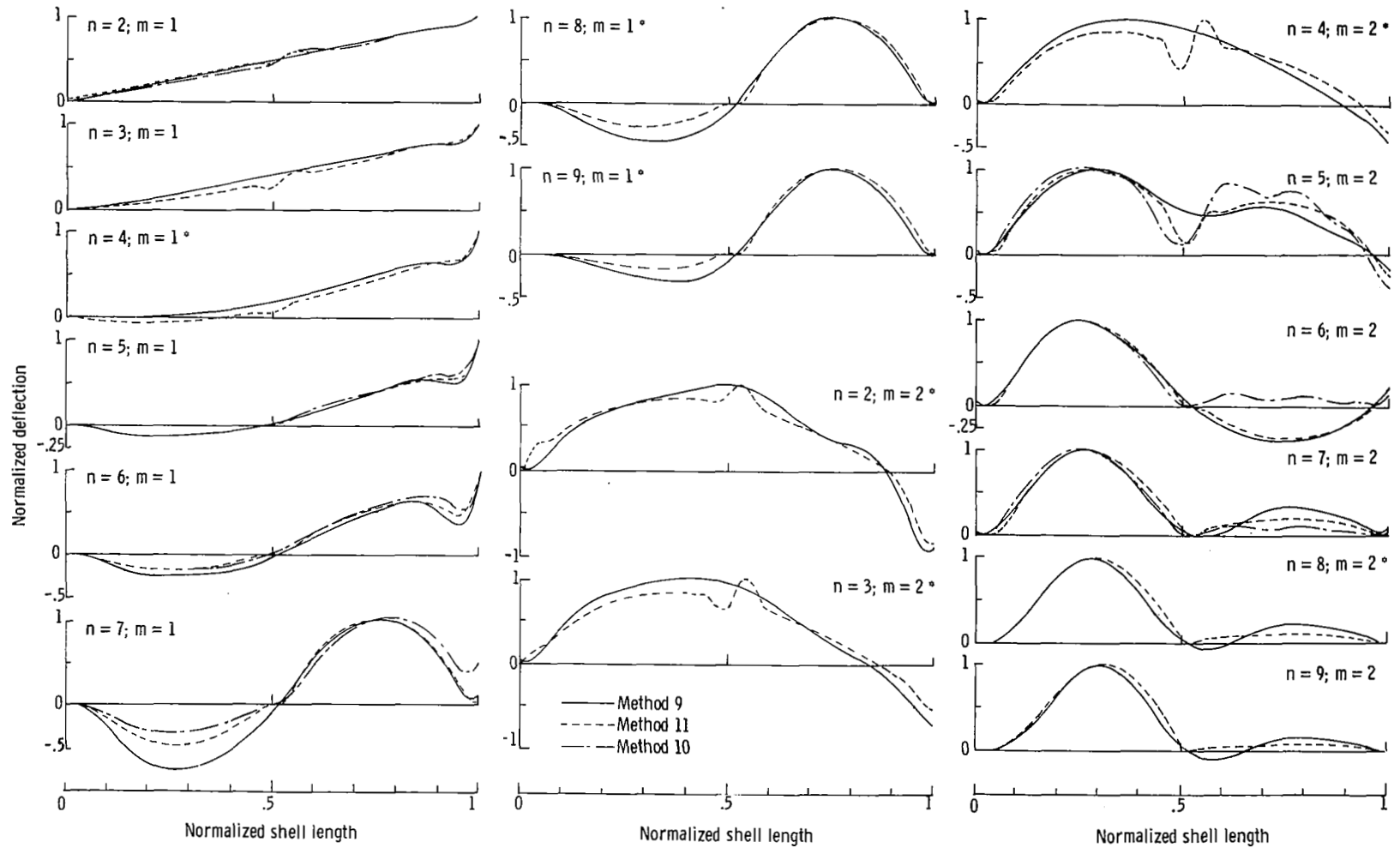


Figure 12.- Comparison of frequency results for model configuration 3C.



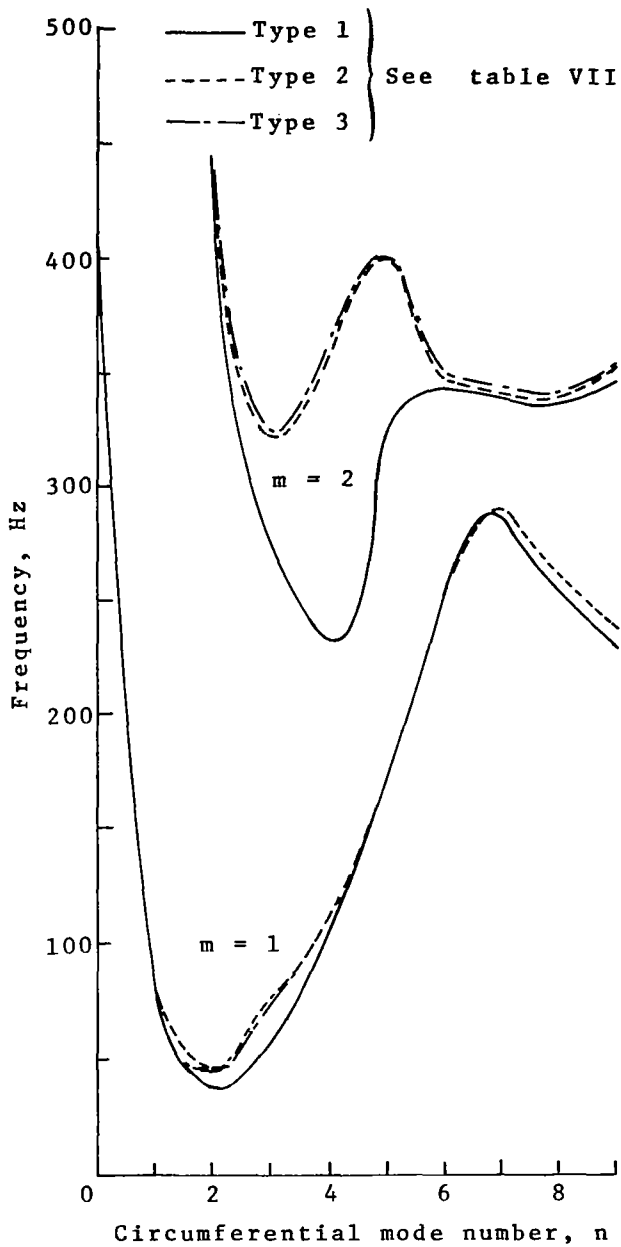
(a) Experimental mode shapes.

Figure 13.- Normalized meridional mode shapes for model configuration 3C.

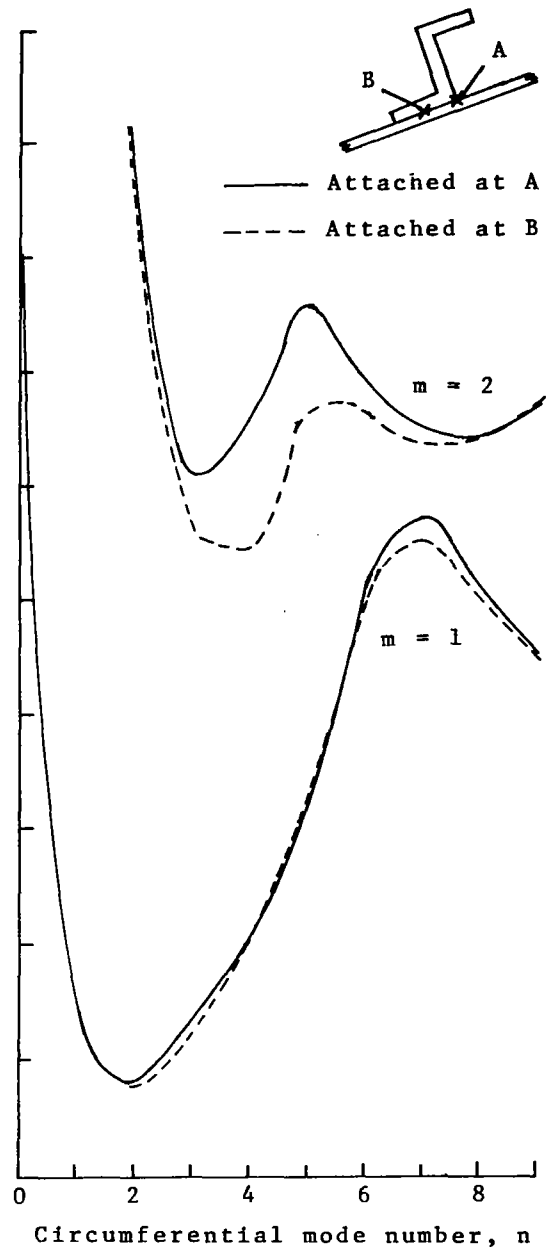


(b) Analytical mode shapes obtained from methods 9, 10, and 11. An asterisk denotes that mode shapes are not available for method 10.

Figure 13.- Concluded.

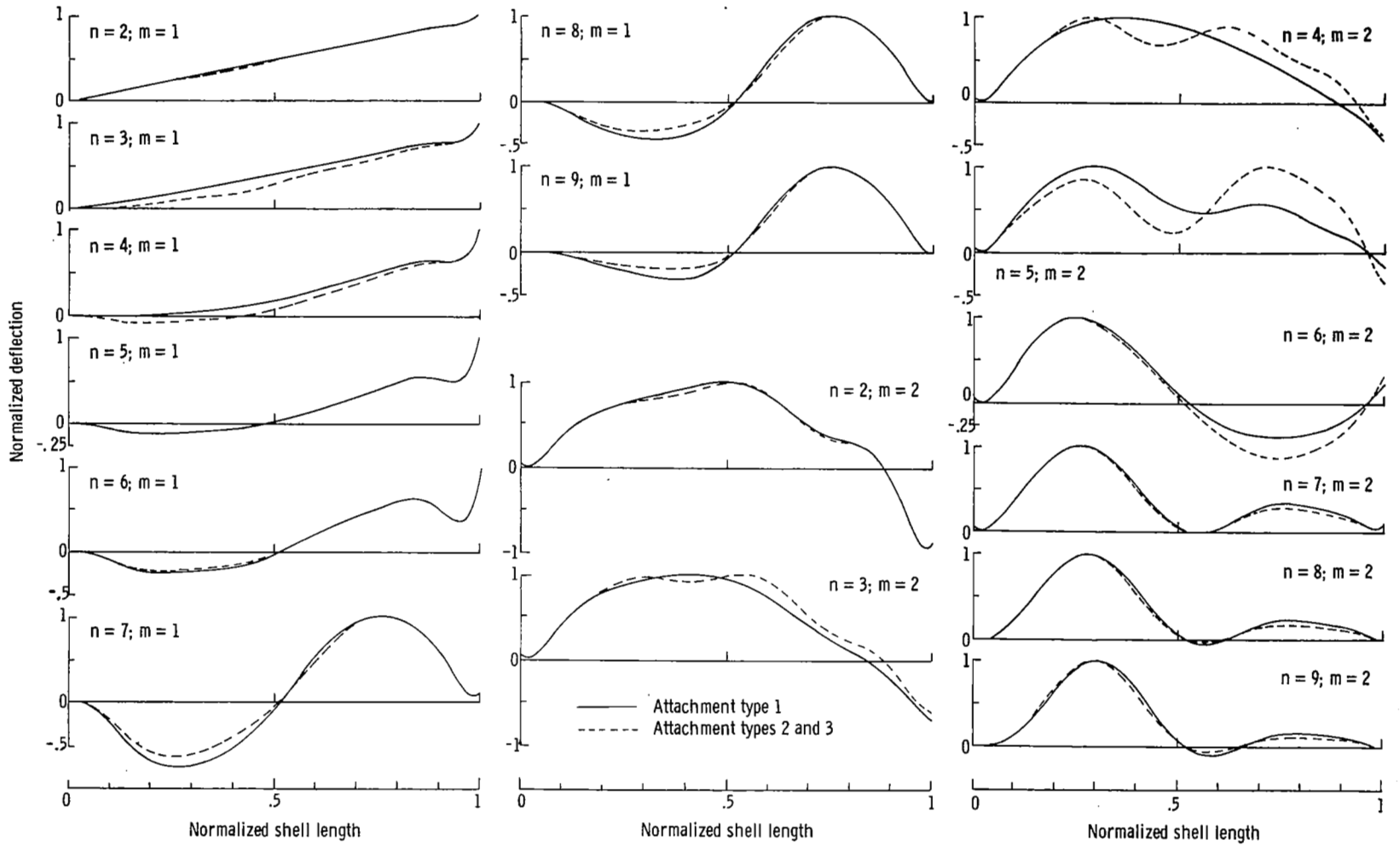


(a) Method 9.



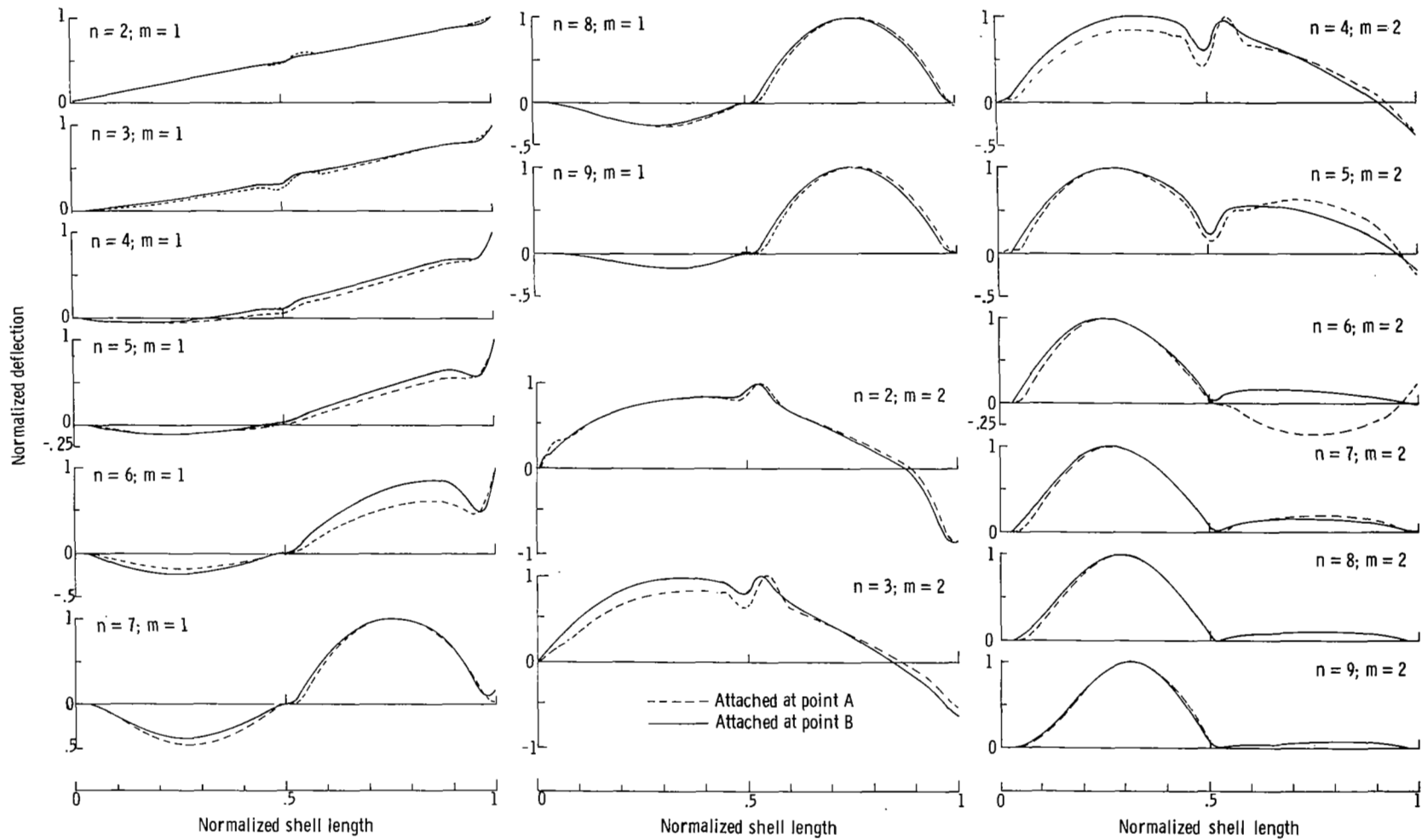
(b) Method 11.

Figure 14.- Frequency results for analytical variations for representing model configuration 3C.



(a) Method 9.

Figure 15.- Calculated meridional mode shapes for model configuration 3C.



(b) Method 11.

Figure 15.- Concluded.

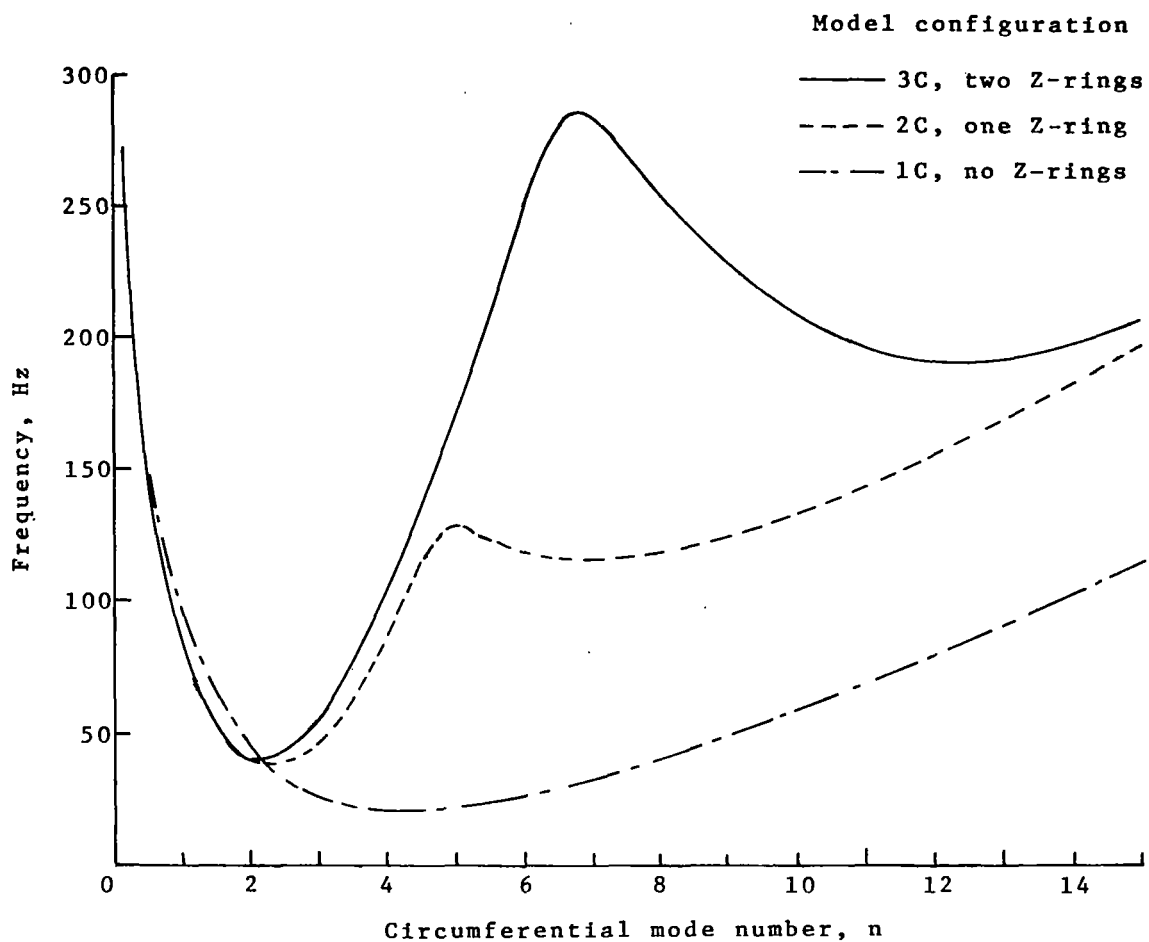


Figure 16.- Calculated first-mode frequencies for model configurations 1C, 2C, and 3C.

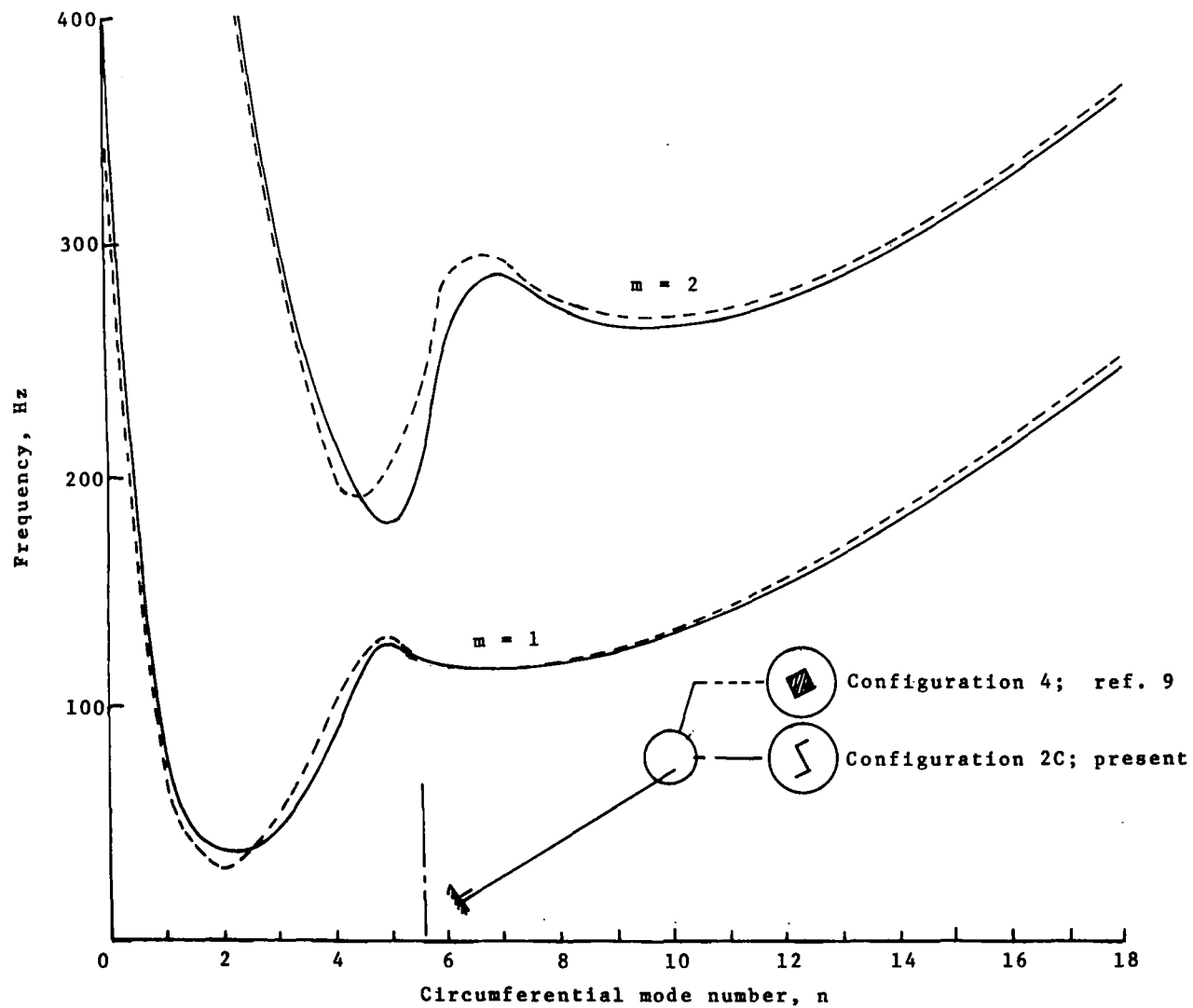


Figure 17.- Comparison of calculated frequencies for models having different ring cross sections.